© 2020. Published by The Company of Biologists Ltd | Journal of Cell Science (2020) 133, jcs246983. doi:10.1242/jcs.246983

RESEARCH ARTICLE

Pex24 and Pex32 are required to tether peroxisomes to the ER for organelle biogenesis, positioning and segregation in yeast

Fei Wu[1,‡], Rinse de Boer[1,‡], Arjen M. Krikken[1], Arman Akşit[1], Nicola Bordin[2,*], Damien P. Devos[2] and Ida J. van der Klei[1,§]

ABSTRACT

The yeast *Hansenula polymorpha* contains four members of the Pex23 family of peroxins, which characteristically contain a DysF domain. Here we show that all four *H. polymorpha* Pex23 family proteins localize to the endoplasmic reticulum (ER). Pex24 and Pex32, but not Pex23 and Pex29, predominantly accumulate at peroxisome–ER contacts. Upon deletion of *PEX24* or *PEX32* – and to a much lesser extent, of *PEX23* or *PEX29* – peroxisome–ER contacts are lost, concomitant with defects in peroxisomal matrix protein import, membrane growth, and organelle proliferation, positioning and segregation. These defects are suppressed by the introduction of an artificial peroxisome–ER tether, indicating that Pex24 and Pex32 contribute to tethering of peroxisomes to the ER. Accumulation of Pex32 at these contact sites is lost in cells lacking the peroxisomal membrane protein Pex11, in conjunction with disruption of the contacts. This indicates that Pex11 contributes to Pex32-dependent peroxisome–ER contact formation. The absence of Pex32 has no major effect on pre-peroxisomal vesicles that occur in *pex3 atg1* deletion cells.

KEY WORDS: Peroxisome, Pex24, Pex32, Endoplasmic reticulum, Membrane contact, Yeast

INTRODUCTION

Peroxins are defined as proteins that play a role in peroxisome biogenesis, including peroxisomal matrix protein import, membrane biogenesis and organelle proliferation (Distel et al., 1996). Most peroxins are peroxisomal or cytosolic proteins that are transiently recruited to the organelle. Recent studies in *Saccharomyces cerevisiae* showed that a family of peroxins, called the Pex23 protein family (Kiel et al., 2006), localize to the endoplasmic reticulum (ER) (David et al., 2013; Joshi et al., 2016; Mast et al., 2016). The function of these peroxins is still poorly understood and is the subject of this study.

Proteins of the Pex23 family are characterized by a DysF domain. The DysF domain was first identified in human dysferlin. Dysferlin is important for fusion of vesicles with the sarcolemma at the site of muscle injury (Bansal and Campbell, 2004; Lek et al., 2011; Bansal et al., 2003). Human dysferlin contains multiple C2 domains, which play a direct role in the above membrane repair process; however, the function of the DysF domain in dysferlin is still obscure.

Yarrowia lipolytica Pex23 was the first DysF-domain-containing peroxin that was identified (Brown et al., 2000). The number of Pex23 family members varies in different yeast species and their nomenclature is confusing (Fig. 1A). *Hansenula polymorpha* and *Pichia pastoris* contain four Pex23 family proteins, but *S. cerevisiae* has five and *Y. lipolytica* has only three. Mutants lacking one of these peroxins show diverse peroxisomal phenotypes ranging from a partial peroxisomal matrix protein import defect to enhanced or decreased peroxisome numbers (Brown et al., 2000; Tam and Rachubinski, 2002; Vizeacoumar et al., 2003, 2004; Yan et al., 2008).

Initially, Pex23 family proteins were thought to localize to peroxisomes (Brown et al., 2000; Tam and Rachubinski, 2002; Vizeacoumar et al., 2003, 2004; Yan et al., 2008). However, later studies indicated that *S. cerevisiae* Pex23 family proteins are ER proteins that form complexes with the ER resident reticulons Rtn1, Rtn2 and Yop1 (David et al., 2013; Mast et al., 2016). *S. cerevisiae* Pex30 and its paralog Pex31 have been implicated in the formation of peroxisome–ER contact sites, where they regulate *de novo* peroxisome formation from the ER (David et al., 2013; Joshi et al., 2016; Mast et al., 2016; Wang et al., 2018). *S. cerevisiae* Inp1 has also been implicated in the formation of peroxisome–ER contacts, but serves a different function, namely in peroxisome retention during yeast budding (Knoblach et al., 2013).

S. cerevisiae Pex30 and Pex31 (ScPex30 and ScPex31) contain a reticulon-like domain and have membrane-shaping properties (Joshi et al., 2016). ER regions where Pex30 accumulates are important for the regulation of pre-peroxisomal vesicle (PPV) formation, but also play a role in lipid droplet biogenesis (Joshi et al., 2018; Wang et al., 2018; Lv et al., 2019).

So far, *S. cerevisiae* Pex29, Pex30 and Pex31 have been extensively studied. However, our knowledge on other members of the *S. cerevisiae* Pex23 protein family, as well as on these proteins from other yeast species, is still relatively scarce.

Here, we studied all four Pex23 family members of the yeast *H. polymorpha*. Our results indicate that these proteins localize to the ER and accumulate at membrane contact sites, including peroxisome–ER contacts and nucleus–vacuole junctions (NVJs). Pex24 and Pex32, but not Pex23 and Pex29, predominantly localize to peroxisome–ER contact sites. Moreover, deletion of *PEX24* or *PEX32*, but not of *PEX23* or *PEX29*, results in major aberrations in peroxisome biology, including defects in peroxisomal matrix protein import and membrane growth, organelle proliferation, positioning and segregation. These defects are accompanied by the disruption of close associations between the peroxisomal and ER membranes, indicating that these proteins are crucial for

[1]Molecular Cell Biology, Groningen Biomolecular Sciences and Biotechnology Institute, University of Groningen, 9300CC Groningen, The Netherlands. [2]Centro Andaluz de Biología del Desarrollo, CSIC, Universidad Pablo de Olavide, Carretera de Utrera, Km.1, Seville 41013, Spain.
*Present address: Structural and Molecular Biology, University College London, London WC1E 6BT, UK.
‡These authors contributed equally to this work

§Author for correspondence (i.j.van.der.klei@rug.nl)

N.B., 0000-0002-6568-9035; D.P.D., 0000-0002-9453-4753; I.J.v.d.K., 0000-0001-7165-9679

Handling Editor: David Stephens
Received 2 April 2020; Accepted 6 July 2020

Journal of Cell Science (2020) 133, jcs246983. doi:10.1242/jcs.246983

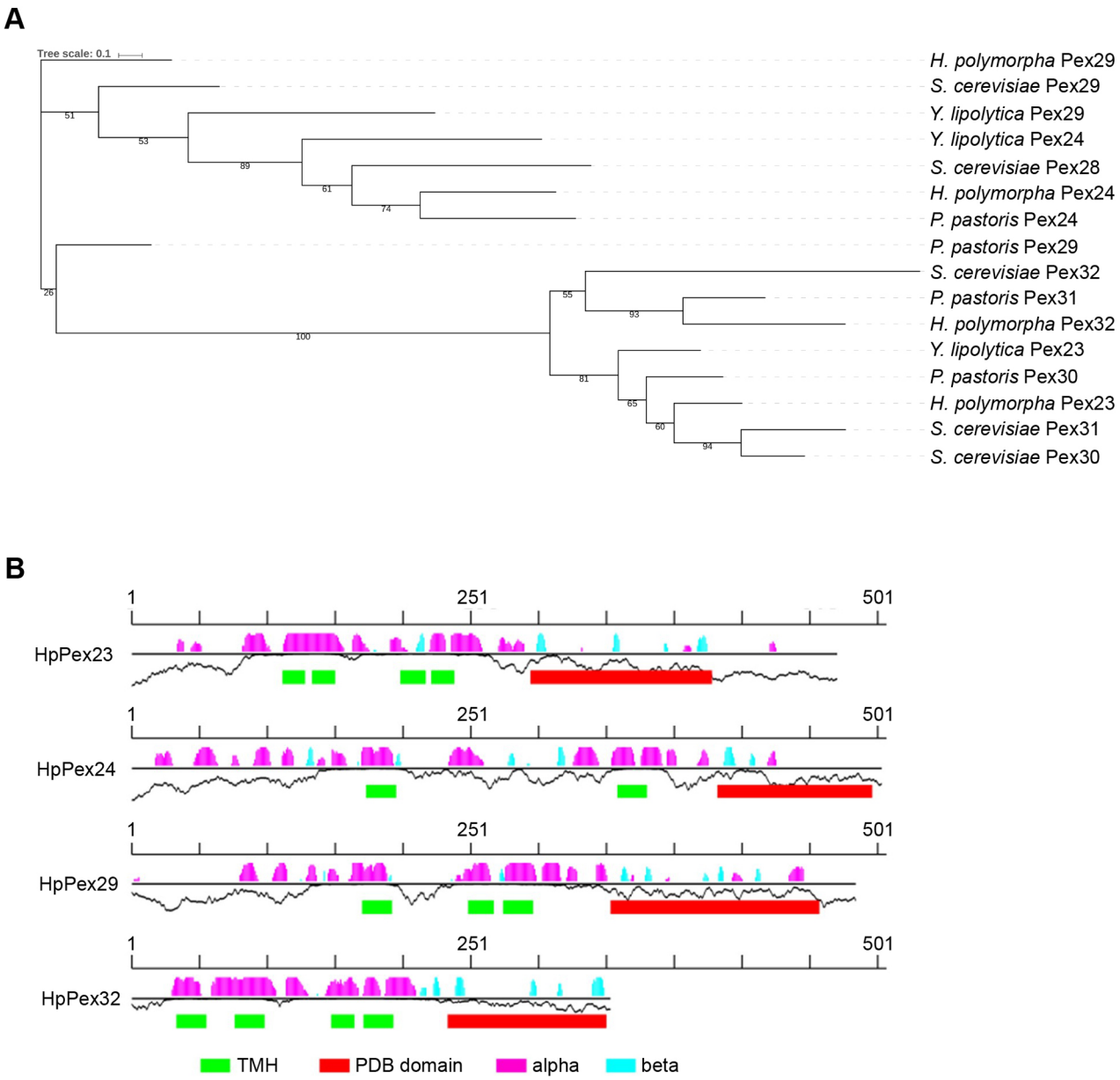

Fig. 1. Yeast Pex23 family proteins. (A) Protein phylogeny. Protein sequences from *S. cerevisiae*, *H. polymorpha*, *P. pastoris* and *Y. lipolytica* were retrieved from the NCBI protein database. Phylogenetic tree: numbers indicate bootstrap values, and branch length represents amino acidic substitution rates. (B) Secondary structure features of *H. polymorpha* Pex23 proteins obtained using the Foundation visualization tool (Bordin et al., 2018). The black horizontal lines represent the protein sequence. The predicted β-strands and α-helices are depicted by bars above each line in cyan and magenta, respectively, with the height of the bars representing the confidence of the prediction. Transmembrane helices (TMH) predictions are depicted as green boxes underneath the secondary structure prediction. The Protein Data Bank (PDB) domain represents the DysF domain.

peroxisome–ER contact site formation. Introduction of an artificial peroxisome–ER tether suppresses the peroxisomal phenotypes, indicating that Pex24 and Pex32 contribute to the tethering of peroxisomes to the ER.

Further studies on the function of Pex32 indicate that the accumulation of this protein at peroxisome–ER contacts is lost in cells lacking the peroxisomal membrane protein Pex11. Moreover, in *pex11* cells peroxisome–ER contacts are defective like in *pex32* cells. These results are consistent with the view that Pex11 is also important for peroxisome–ER associations. Deletion of *PEX32* in *pex3 atg1* cells did not result in a change in the abundance or morphology of PPVs, suggesting that Pex32 is not involved in the regulation of PPV formation.

RESULTS

Protein sequence and structure prediction

Construction of a phylogenetic tree of Pex23 family members from four different yeast species indicated that two subfamilies (the Pex23 and Pex24 subfamilies) can be distinguished (Fig. 1A). All *H. polymorpha* members contain a DysF domain at the C terminus. *H. polymorpha* Pex32 (HpPex32) is much shorter than the other family members, which is mostly due to the lack of an unstructured fragment at the amino terminus of this protein (Fig. 1B).

HpPex23 ends with a Lys-Lys-Lys-Glu stretch of residues, similar to the Lys-Lys-Xaa-Xaa (where Xaa indicates any amino acid) found in *S. cerevisiae* Pex30 (David et al., 2013), whereas HpPex24 ends with Lys-Lys-Arg. These C termini might represent

Journal of Cell Science (2020) 133, jcs246983. doi:10.1242/jcs.246983

di-lysine motifs, which are recognized by coatomer subunits and important for retrograde transport to the ER (Ma and Goldberg, 2013). The C termini of HpPex29 and HpPex32 do not contain di-lysine motifs.

Secondary structure prediction indicated that all four sequences contain between two to four transmembrane helices and a C-terminal domain dominated by β-sheets (Fig. 1B). It has been previously argued that a reticulon-like domain was observed in this family of proteins, particularly in ScPex30 and ScPex31 (Joshi et al., 2016). Indeed, a similar domain prediction can be found for HpPex23 using HHpred on the Pfam-A database. This detection extends from residue 100 to 233 of HpPex23. However, this detection has an Expect value (E-value) of 2 and a probability of 92.38, making it a borderline detection. Similar borderline domain predictions are detected for HpPex24, HpPex29 and HpPex32. A Trp residue is also present at the N terminus of this potential domain and aligns with the classically conserved Trp residue of other Pex reticulon-like domains.

All *H. polymorpha* Pex23 family members localize to the ER

The localization of the four *H. polymorpha* Pex23 family proteins was determined using fluorescence microscopy (FM) using strains producing C-terminally GFP-tagged proteins under control of their endogenous promoters (Fig. 2A,B). Functional peroxisomes are essential for growth of *H. polymorpha* on methanol. All four strains grew similarly to the wild-type (WT) control on medium containing methanol, indicating that tagging with GFP at the extreme C terminus does not affect the function of Pex23 family proteins in peroxisome biology (Table S1).

Protein localization was assessed using cells that were grown in medium containing glucose (peroxisome-repressing conditions). In these conditions the cells generally contain a single small peroxisome that is associated with the ER (Wu et al., 2018). As shown in Fig. 2B, all four proteins colocalized with the ER marker BiP–mCherry–HDEL, predominantly at the cortical ER. Frequently, a patch of Pex23–GFP was observed at the nuclear envelope as well (Fig. 2A,B). In Pex24–GFP- or Pex32–GFP-producing strains generally one fluorescent spot was detected per cell, which invariably localized close to the single peroxisome marked with Pex14–mKate2. More fluorescent spots were present in cells of Pex23–GFP- and Pex29–GFP-producing strains, and one of them invariably was present in the vicinity of the Pex14–mKate2 spot (Fig. 2A).

Upon overproduction, all four *H. polymorpha* Pex23 family proteins showed a typical cortical ER and nuclear envelope pattern of localization, supporting that they represent genuine ER proteins. FM analysis revealed that the overproduced proteins were not evenly distributed over the ER, but were present in spots and patches. In all strains, one cortical patch localized in the vicinity of the peroxisome (here marked with DsRed–SKL) (Fig. 2C). Relatively large patches of GFP fluorescence were frequently observed at the nuclear envelope in cells overproducing Pex24–GFP. Colocalization studies with the nucleus–vacuole junction (NVJ) protein Vac8 indicated that these patches represent NVJs (Fig. 2D). Pex23–GFP also accumulated at NVJs when produced under control of its own promoter.

Western blot analysis showed that the levels of all four GFP fusion proteins were very low when produced under control of their endogenous promoters. In fact, Pex24–GFP and Pex32–GFP were below the limit of detection, whereas faint bands were detected on blots of lysates from Pex23–GFP- and Pex29–GFP-producing cells. Upon overproduction, all four GFP-fusion proteins were readily detected (Fig. 2E).

Our data support observations in *S. cerevisiae*, where Pex23 family proteins localize to the ER, including at regions where peroxisomes and the ER are in close vicinity (David et al., 2013; Mast et al., 2016). The presence of a proportion of HpPex23 and overproduced HpPex24 at NVJs suggests that Pex23 family proteins are also components of other membrane contacts.

The absence of Pex24 and Pex32 affects peroxisome biogenesis and abundance

To study the role of the Pex23 family proteins we constructed four *H. polymorpha* deletion strains, *pex23*, *pex24*, *pex29* and *pex32*. First, we analyzed whether Pex23 family proteins are important for peroxisomal matrix protein import in glucose-grown cells producing the matrix marker GFP–SKL using widefield fluorescence microscopy (FM). GFP–SKL mislocalized to the cytosol in a proportion of the *pex32* cells (Fig. 3A), whereas cytosolic fluorescence was occasionally observed in *pex23* and *pex24* cells, but never in *pex29* cells. In *pex32* cultures, typically three types of cells could be discriminated, namely: (1) cells with a GFP spot without cytosolic fluorescence, (2) cells with a GFP spot in conjunction with cytosolic GFP and (3) cells with only cytosolic GFP. This indicates that although matrix protein import is strongly compromised in some of the cells, Pex32 is not essential for the assembly of a functional importomer.

Next, we quantified the number of GFP containing spots using confocal laser scanning microscopy (CLSM) and a custom-made plugin for ImageJ (Thomas et al., 2015). In these images, cytosolic fluorescence was not detected in any of the strains due to the lower sensitivity of CLSM relative to widefield FM. The average number of GFP spots per cell was similar in WT and *pex29* cells but reduced in the other three deletion strains. The strongest reduction was observed in *pex24* and *pex32* cells (Fig. 3B). Frequency distributions show that these reductions are accompanied by an increase in the percentage of cells lacking a GFP spot (Fig. 3B). These results indicate that Pex24 and Pex32 are important for normal peroxisome abundance.

Finally, we analyzed the strains in peroxisome-inducing growth conditions (methanol). Mislocalization of peroxisomal matrix enzymes affects methylotrophic growth (van der Klei et al., 2006). We therefore routinely grow peroxisome-deficient mutants on a mixture of glycerol and methanol (Knoops et al., 2014). At these conditions, cells grow on glycerol (which does not require peroxisome function), while methanol is used as additional carbon and energy source, depending on the severity of the peroxisome function defect. Growth experiments using glycerol-methanol medium revealed that the strongest growth defects were in the *pex32* and *pex24* strains. Cells of the *pex23* strain showed only a minor reduction in growth, whereas *pex29* cells grew similar to WT controls (Fig. 3D). These data indicate that the function of peroxisomes is strongly compromised in the absence of Pex24 and Pex32, but not in cells lacking Pex29.

Quantification of structures marked with the *H. polymorpha* peroxisomal membrane marker Pmp47–GFP (Cepińska et al., 2011) indicated that in these growth conditions, relative to WT controls, peroxisome abundance was reduced, especially in *pex24* and *pex32* cells (Fig. 3C). Moreover, CLSM revealed that *pex23*, *pex24* and *pex32* cells frequently contained a peroxisome of enhanced size (Fig. 3C).

In conclusion, *pex24* and *pex32* cells showed the most severe peroxisomal phenotypes, whereas *pex29* cells were similar to WT and *pex23* cells had minor peroxisomal defects.

Journal of Cell Science (2020) 133, jcs246983. doi:10.1242/jcs.246983

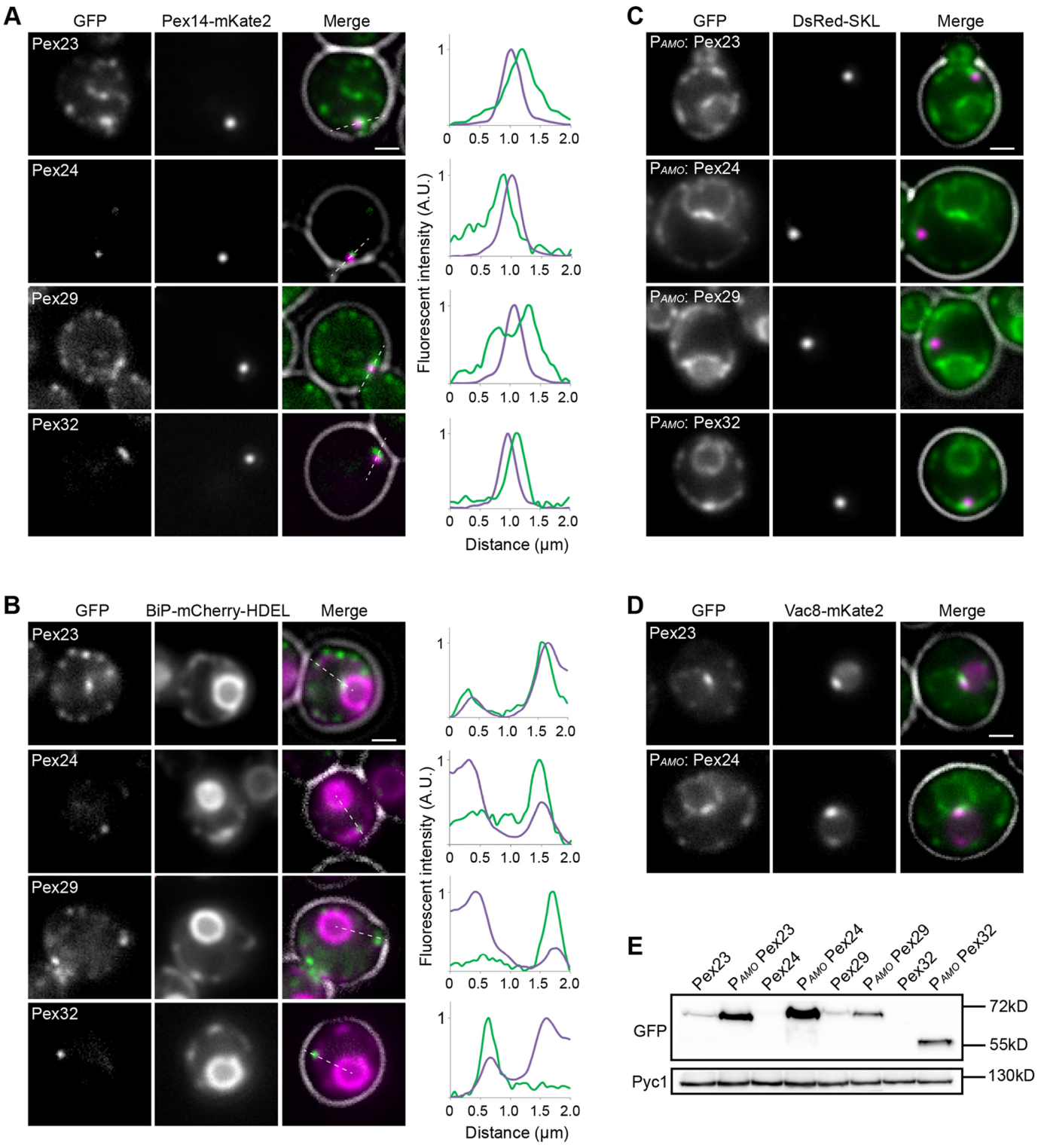

Fig. 2. *H. polymorpha* Pex23 family proteins localize to the ER. (A,B) FM images of glucose-grown *H. polymorpha* cells producing the indicated GFP fusion proteins under control of their endogenous promoters together with the peroxisomal marker Pex14–mKate2 (A) or the ER marker BiP–mCherry–HDEL (B). The merged images show the cell contours in white. Graphs show relative fluorescence intensity of GFP (green) and mKate2 or mCherry (purple), measured along the dotted lines shown in the merge images. Representative images of two experiments are shown. (C) FM images of glucose-methylamine-grown *H. polymorpha* WT cells producing the peroxisomal marker DsRed–SKL and the indicated GFP fusion proteins under control of the amine oxidase promoter (P_{AMO}). Representative images of two experiments are shown. (D) Colocalization of Vac8–mKate2 with Pex23–GFP produced under control of the endogenous promoter, or Pex24–GFP expressed under control of P_{AMO}. Representative images of two experiments are shown. (E) Western blot analysis of the indicated strains. Cells were grown for 4 h on glucose. Strains producing the GFP fusion proteins under control of P_{AMO} were grown in medium containing methylamine as nitrogen source. Equal amounts of cellular lysates were loaded per lane. Blots were decorated with α-GFP or α-Pyruvate carboxylase 1 (Pyc1) antibodies. Pyc1 was used as a loading control. A representative blot of three experiments is shown. Scale bars: 1 μm.

Journal of Cell Science (2020) 133, jcs246983. doi:10.1242/jcs.246983

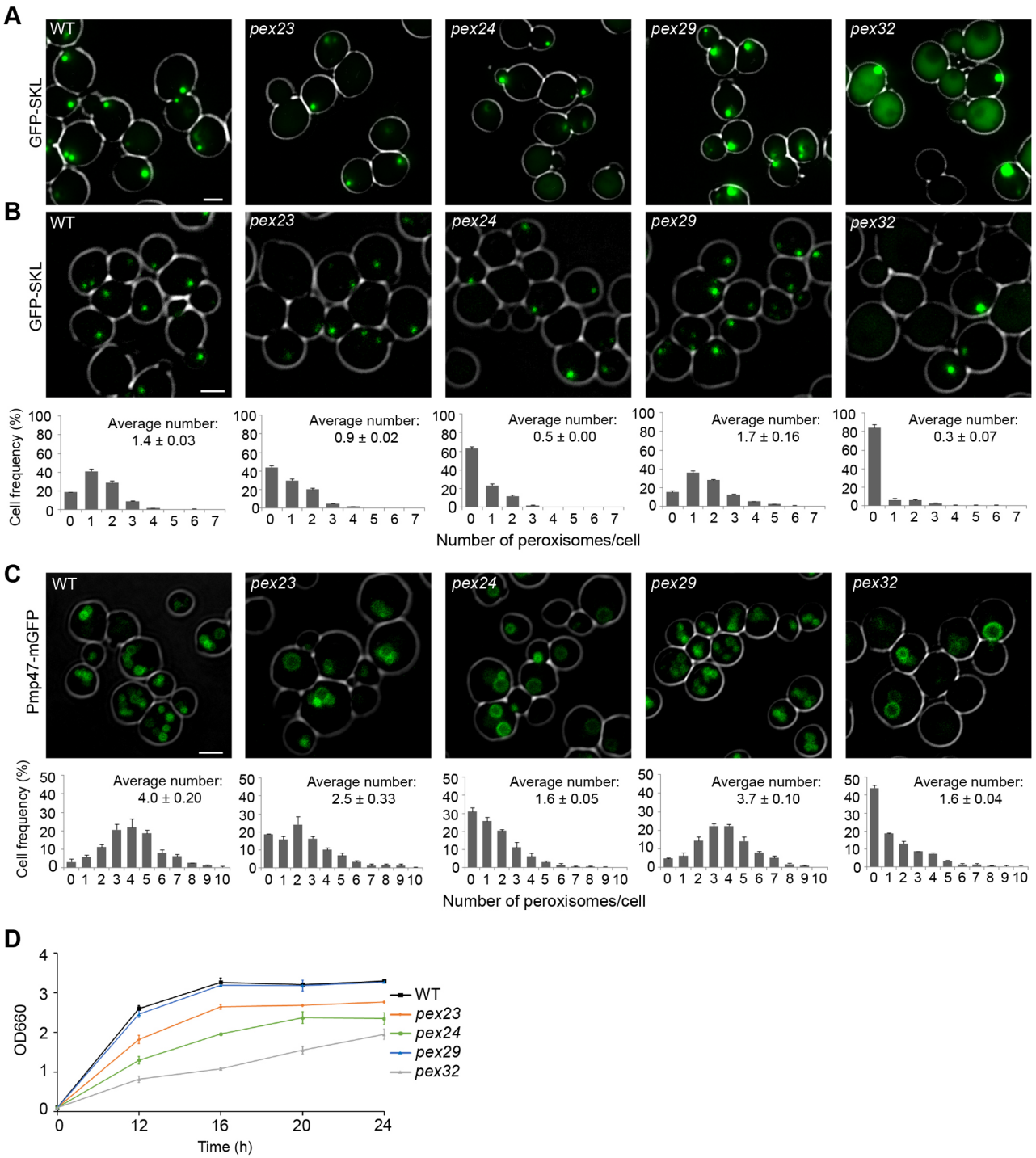

Fig. 3. Deletion of *PEX23*, *PEX24* or *PEX32* results in aberrant peroxisome formation. FM (A) and CLSM (B) images in conjunction with peroxisome quantification of the indicated deletion strains producing the peroxisome matrix protein GFP–SKL and grown on glucose. Data are mean±s.d. of two independent experiments (n=2 using 500 cells from each experiment). (C) CLSM images of Pmp47–GFP-producing cells grown on a mixture of glycerol and methanol. Data are mean±s.d. of two independent experiments (n=2 using 300 cells from each experiment). In the upper right corners of the graphs, the average number of peroxisomes per cell is indicated. Data are mean±s.d. of two independent experiments (n=2 using 300 cells from each experiment). (D) Growth curves of the indicated strains in medium containing a mixture of glycerol and methanol. The optical density (y-axis) is expressed as absorbance at 660 nm (OD_{660}). Data are mean±s.d. of two independent cultures. Scale bars: 2 µm.

The absence of Pex23 family proteins disrupts peroxisome–ER contacts

In *S. cerevisiae*, Pex23 family proteins and Inp1 play a role in the formation of peroxisome–ER contacts (David et al., 2013; Knoblach et al., 2013; Mast et al., 2016). By measuring the distance between peroxisomal and ER membranes in electron micrographs, we analyzed the role of *H. polymorpha* Pex23 proteins in the formation of peroxisome–ER contacts (Fig. 4). At membrane contact sites, the two membranes are usually separated by a distance smaller than 30 nm. As shown in Fig. 4A, in WT controls the distance between

Journal of Cell Science (2020) 133, jcs246983. doi:10.1242/jcs.246983

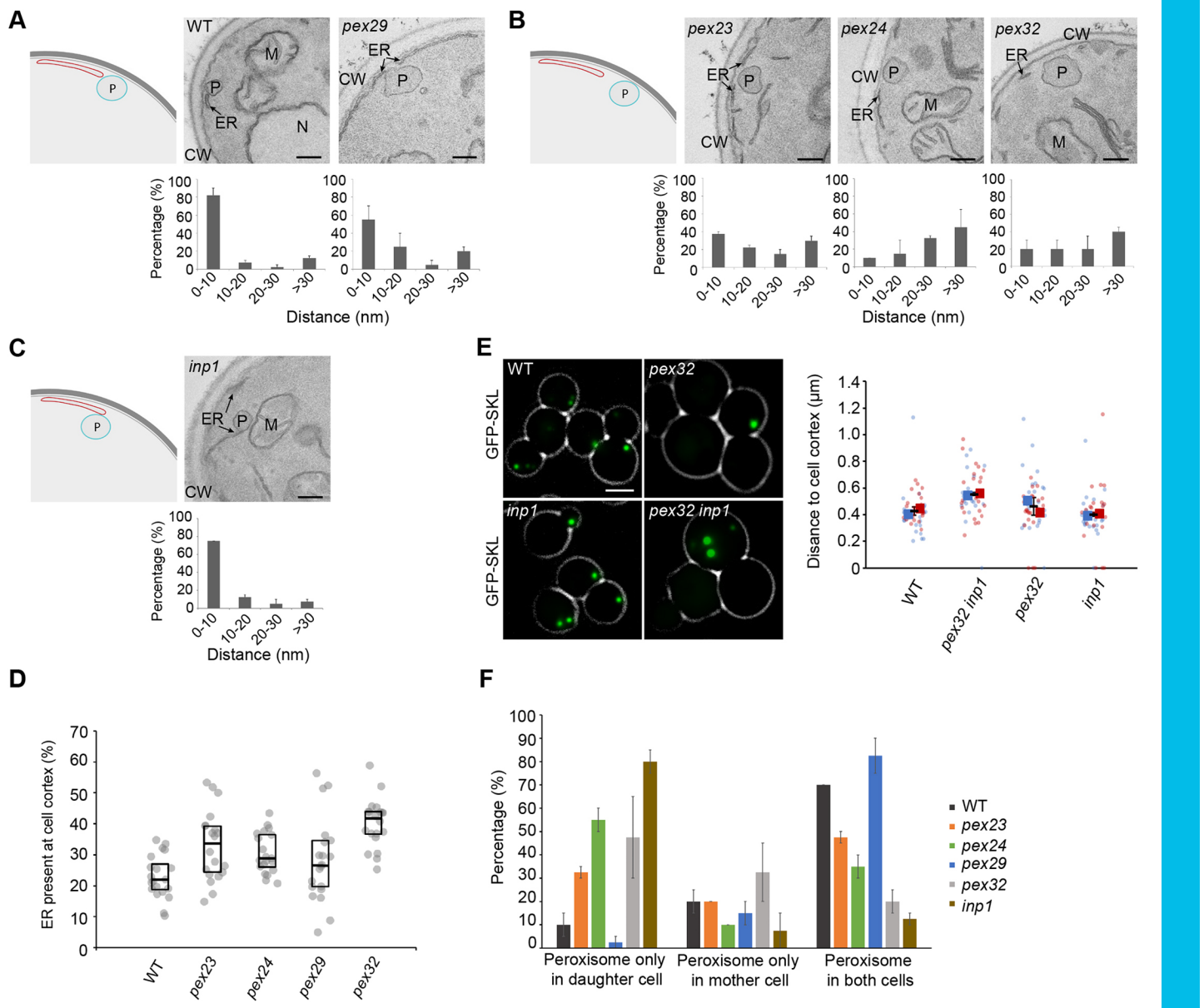

Fig. 4. Deletion of *PEX23*, *PEX24* or *PEX32* results in an increase in distance between peroxisomal and ER membranes. (A–C) Illustrative diagrams and EM images of thin sections of $KMnO_4$-fixed glucose-grown cells of the indicated strains, and quantification of the distance between the ER and peroxisomal membranes. Data are mean±s.d. of two independent experiments (*n*=2 based on 21 peroxisomes in random sections from each experiment). CW, cell wall; ER, endoplasmic reticulum; P, peroxisome; M, mitochondrion; N, nucleus. Scale bars: 200 nm. (D) Quantification of ER abundance at the cell cortex. The percentage of the cell cortex covered by the ER was measured in 20 random cell sections using EM. For each strain, the ER coverage is depicted as an interquartile box together with the percentages of the individual cells. (E) FM images and a SuperPlot showing the distance between the GFP spot and the cell cortex in the indicated strains producing GFP–SKL. *n*=2 using 24 cells from each biological replicate. The duplicate experiments are color coded. The circles represent the single data points. The squares are the mean from each experiment and the error bars indicate the s.d. (F) Quantification of the presence of peroxisomes in both the mother cell and bud in the indicated mutants. Data are mean±s.d. from two independent experiments (*n*=2 using 20 peroxisome-containing budding yeast cells from each experiment).

both membranes was generally less than 10 nm for ∼80% of the peroxisomal profiles analyzed, whereas the distance was larger than 30 nm in less than 10% of the profiles analyzed (Fig. 4A). In cells of the *pex23* and *pex29* strains, only 40% of the organellar profiles had a measured distance of less than 10 nm, and this percentage further dropped for *pex24* and *pex32* cells to 10–20% (Fig. 4A,B). These changes were not related to a decrease in total cortical ER, which instead slightly increased (Fig. 4D). Deletion of *INP1* had no effect on the distance at peroxisome–ER contact sites (Fig. 4C), in line with our recent observation that *H. polymorpha* Inp1 associates peroxisomes to the plasma membrane (Wu, 2020). Based on these observations, we conclude that Pex24 and Pex32 – and to a lesser extent Pex29 and Pex23, but not Inp1 – play crucial roles in the formation of tight membrane contacts between peroxisome and ER membranes.

In glucose-grown WT cells, the single peroxisome is invariably localized at the cell cortex. FM analysis of the position of peroxisomes demonstrated that peroxisomes remained close to the cell cortex upon deletion of either *PEX32* or *INP1*. However, in a *pex32 inp1* double mutant, peroxisomes were more frequently

Journal of Cell Science (2020) 133, jcs246983. doi:10.1242/jcs.246983

observed in the central part of the cells, indicating that Pex32 and Inp1 together contribute to the cortical association of peroxisomes (Fig. 4E).

In budding WT cells, at least one peroxisome is retained in the mother cells, whereas another one is transported to the nascent bud. Quantification of peroxisomes in mother cells and buds indicated that the organelles normally segregated between mother cells and buds of the *pex29* strain, similar to segregation observed in WT controls. Cultures of *pex23*, *pex24* and *pex32* cells, however, showed aberrant peroxisome segregation patterns. In *pex24* cultures, a large fraction of the budding cells contained peroxisomes solely in the buds, indicative of a defect in retention of peroxisomes in mother cells (Fig. 4F). A similar, but stronger retention defect was observed in *inp1* control cells, known to be defective in peroxisome retention (Fig. 4F).

Our data show that close associations between peroxisomes and the ER require Pex23 family proteins, of which Pex24 and Pex32 are paramount. Inp1 is not crucial for the formation of these associations. Our data furthermore show that these associations contribute to peroxisome positioning at the cell cortex and proper peroxisome segregation in budding cells.

An artificial peroxisome–ER tether suppresses the peroxisomal phenotypes

To study whether the effect of the absence of Pex24 and Pex32 on peroxisome biology is due to the loss of peroxisome–ER contacts, we introduced an artificial tether in an attempt to reassociate both organelles. This approach is based on studies in *S. cerevisiae*, in which the absence of proteins of the ER–mitochondria encounter structure (ERMES) is partially complemented by artificially anchoring mitochondria to the ER (Kornmann et al., 2009). To this end we constructed an artificial tether protein consisting of full-length Pex14 and the tail anchor of the ER protein Ubc6, separated by two heme-agglutinin tags (HA). This construct (P_{ADH1}Pex14–HA–HA–Ubc6^{TA}), termed ERPER, was introduced in WT and the four deletion strains (Fig. 5A). Electron microscopy (EM) showed that introduction of ERPER resulted in regions of close apposition (<10 nm) between the ER/nuclear envelope and the peroxisomal membranes (Fig. 5B,C). Immuno-EM using anti-HA antibodies confirmed the presence of ERPER tether protein at these regions (Fig. 5B). EM also showed that, upon growth on a mixture of methanol and glycerol, multiple peroxisomes were present in all mutant strains producing ERPER, as was also the case in WT controls producing ERPER (Fig. 5C), an observation that was confirmed by FM (Fig. 5D). Furthermore, in *pex32* cells producing both ERPER and GFP–SKL, cytosolic fluorescence was not detectable (Fig. 5D), indicating that the matrix protein import defect was suppressed by ERPER. Peroxisome quantification showed that peroxisome numbers in *pex24* and *pex32* cells containing ERPER were similar to those in WT control cells producing ERPER (Fig. 5E; compare with Fig. 3C).

Introduction of ERPER did not affect the growth of WT, whereas it partially suppressed the growth defects that were observed for the *pex24* and *pex32* deletion strains on glycerol-methanol medium (Fig. 5F), confirming that the tether restored peroxisome matrix protein import and peroxisome function. As expected, the tether did not affect growth of *pex29* cells on methanol (Fig. S1B). Furthermore, the minor growth defect of *pex23* was not suppressed by ERPER, suggesting that this defect is not caused by altered peroxisome–ER contacts (Fig. S1C).

Introduction of a control construct containing P_{ADH1}Pex14, which does not cause tethering of peroxisomes to the ER, did not alter peroxisome biogenesis or function in WT cells (Fig. S1A). Only introduction of ERPER (P_{ADH1}Pex14–HA–HA–Ubc6^{TA}), and not overexpression of Pex14 under the same promoter (P_{ADH1}Pex14; Pex14++), suppressed the growth defect of *pex32* cells on glycerol-methanol, confirming that artificial tethering and not solely the enhanced Pex14 levels are responsible for suppression of the phenotype (Fig. S1D).

From this we conclude that the severe peroxisome defects in *pex24* and *pex32* cells are related to a loss in tight peroxisome–ER contacts.

Pex24 and Pex32 are important for peroxisomal membrane growth

Membrane contacts of cell organelles with the ER have been implicated in lipid transfer. To test whether the Pex24- and Pex32-dependent peroxisome–ER contacts are important for expansion of peroxisomal membranes, we compared the average peroxisomal membrane surface per cell in the four deletion strains relative to the WT control. A plug-in for the analysis of CLSM images allows quantification of the average diameter of peroxisomes by fitting spheres in data obtained from the green channel of combined *z*-slices of glycerol-methanol grown, Pmp47–GFP-producing cells (Thomas et al., 2015). From these data we estimated the average peroxisomal membrane surface per cell. As shown in Fig. 5G, these values were reduced in *pex24* and *pex32* cells relative to values for *pex23*, *pex29* and WT cells. Because we are aware of the drawbacks of analyzing organelle sizes by FM (the limited resolution of FM may cause an overestimation of the diameter of very small organelles that are more abundant in WT cells), we also quantified the average length of peroxisomal membranes in cell sections using EM (Fig. 5H). This analysis confirmed that in *pex32* cells especially, but also in *pex24* cells, the peroxisomal membrane surface is reduced.

Similar analyses of the *pex24* and *pex32* strains containing ERPER showed that the average peroxisome membrane surface area per cell was increased (Fig. 5G,H), suggesting that Pex24- and Pex32-dependent contacts might contribute to lipid supply and hence peroxisomal membrane expansion.

Pex23, Pex24 and Pex29 are not functionally redundant with Pex32

Because *pex32* cells showed the strongest peroxisome phenotype, we confined our further studies to Pex32. First, we analyzed whether the phenotype of *pex32* cells could be suppressed by overproduction of any of the other members of the Pex23 protein family. To this purpose, the corresponding genes were placed under control of the strong amine-inducible amine oxidase promoter (P_{AMO}). Quantitative analysis of FM images of glucose-methylamine-grown cells indicated that upon overexpression of *PEX32* in *pex32* cells peroxisome numbers increased. This was not the case upon overexpression of *PEX23*, *PEX24* or *PEX29* (Fig. 6A). Similarly, overexpression of *PEX32*, but not of *PEX23*, *PEX24* or *PEX29*, almost completely restored the growth defect of *pex32* cells on methanol (Fig. 6B). These data show that *PEX23*, *PEX24* and *PEX29* are not functionally redundant with *PEX32*.

Pex32–GFP concentrates at peroxisome–ER membrane contact sites

Next, we performed correlative light and electron microscopy (CLEM) to analyze Pex32–GFP localization at high resolution. In order to obtain sufficient fluorescence signal, Pex32–GFP was slightly overexpressed by placing the gene under control of the

Journal of Cell Science (2020) 133, jcs246983. doi:10.1242/jcs.246983

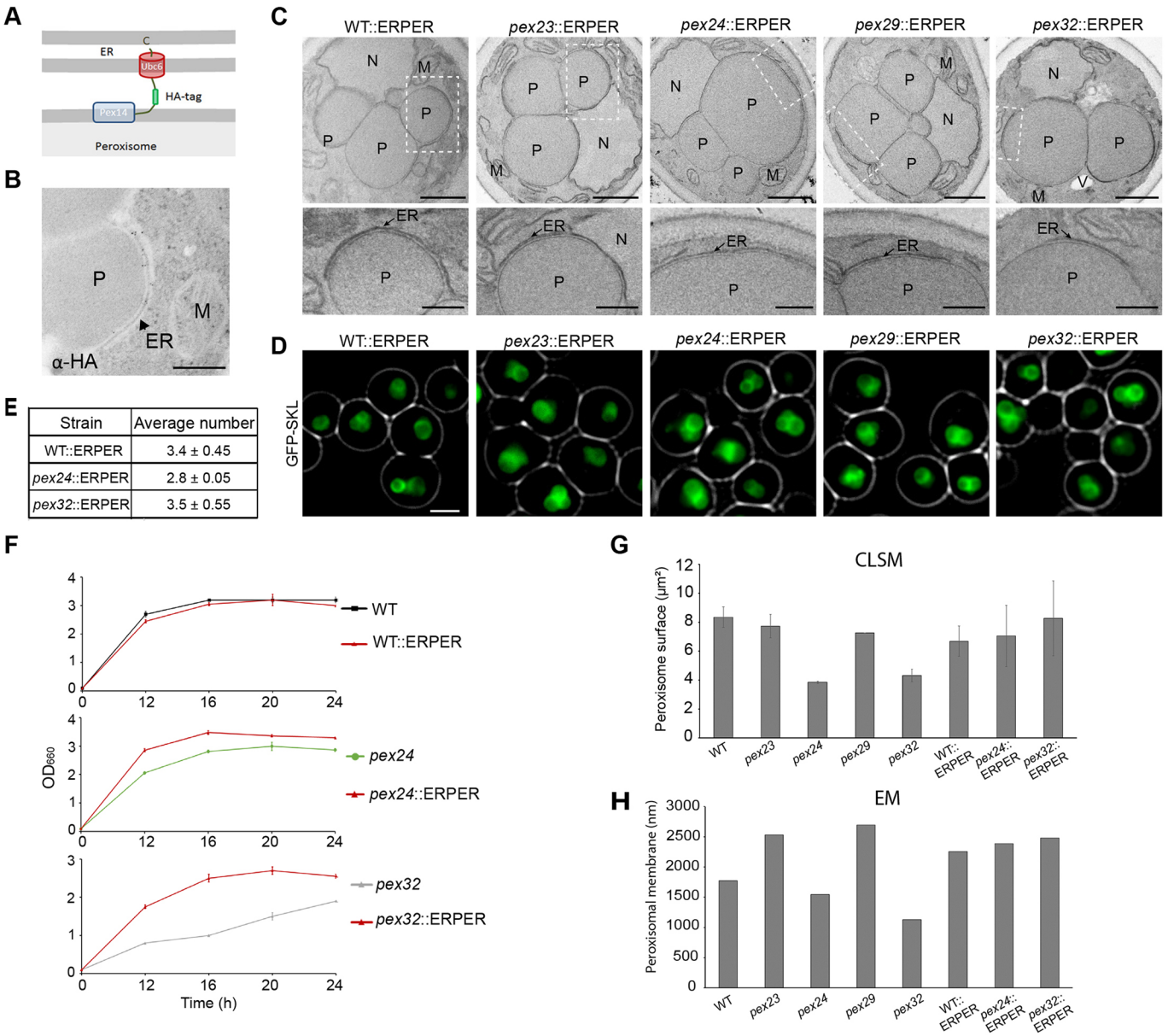

Fig. 5. Suppression of peroxisome defects by an artificial peroxisome–ER tether. (A) Schematic representation of the ERPER tethering. (B) Immunolabeling using HA antibodies of a WT P_{ADH1}*PEX14–HAHA–UBC6* cell. M, mitochondrion; P, peroxisome; ER, endoplasmic reticulum. Cells were embedded for EM once and the labeling was performed twice. Scale bar: 200 nm. (C) EM images of $KMnO_4$-fixed cells of the indicated mutant strains expressing ERPER. Scale bars: 500 nm (top), 200 nm (bottom). Cells were embedded for EM once. Dashed boxes in top images indicate regions shown magnified below. (D) FM analysis of the indicated strains grown on glycerol-methanol medium and producing GFP–SKL. Because peroxisomes harbor an alcohol oxidase crystalloid, GFP is not evenly distributed over the peroxisomal matrix. Representative images from two experiments are shown. Scale bar: 2 µm. (E) Quantification of peroxisome numbers based on CLSM analysis of methanol–glycerol grown PMP47–GFP-producing cells of the indicated mutant strains containing ERPER. Data are mean±s.d. *n*=2 using 300 cells from two independent cultures. (F) Growth curves of the indicated strains on glycerol-methanol medium. The optical density (*y*-axis) is expressed as absorbance at 660 nm (OD_{660}). Data are mean±s.d. from two independent cultures. (G) Average cellular peroxisome surface area calculation based on CLSM images of methanol-glycerol-grown cells of the indicated strains. Data are mean±s.d. from two independent experiments (*n*=2 using 300 cells from each experiment). (H) Quantification of the average abundance of peroxisomal membranes in 50 EM cell sections of the indicated strains from a single experiment.

P_{AMO} promoter and inducing expression for a short period. Under these conditions, generally only a single fluorescent spot was detected per cell. EM analysis revealed that the fluorescent spot characteristically localized at the region where the ER and peroxisomal membrane were closely associated (Fig. 6C). In total, four tomograms were analysed, and in all of them the Pex32–GFP-dependent fluorescent spot was present at the peroxisome–ER contact site.

Pex11 is required for the formation of peroxisome–ER contact sites and the concentration of Pex32–GFP at these sites

Next, we examined whether the peroxisome–ER association is required for concentrating Pex32. To address this, we localized Pex32–GFP in a *pex3 atg1* double deletion strain, which lacks normal peroxisomes but contains PPVs (Knoops et al., 2014). In these cells Pex32–GFP accumulation in a spot was lost. Instead, multiple fainter Pex32–GFP spots were observed (Fig. 6D). In a

Journal of Cell Science (2020) 133, jcs246983. doi:10.1242/jcs.246983

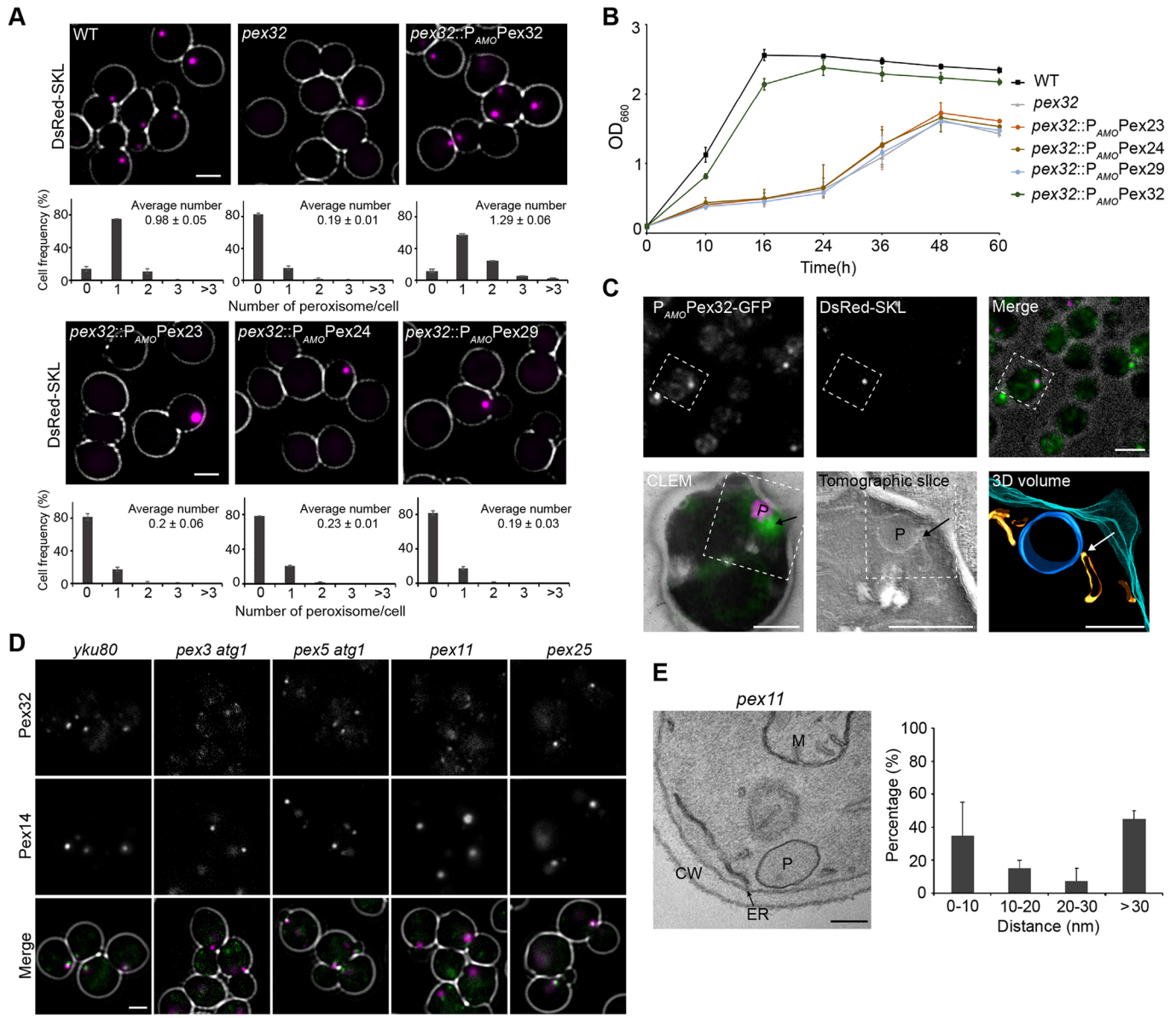

Fig. 6. Specific Pex32 localization depends on Pex3 and Pex11. (A) FM images and peroxisome quantification of glucose-grown WT and *pex32* cells with or without overproduction of the indicated proteins. Peroxisomes are marked with DsRed–SKL. Data shown are mean±s.d. from two independent experiments (*n*=2 using 200 cells from each experiment). Scale bars: 2 µm. (B) Growth curves of the indicated strains in medium containing a mixture of glycerol and methanol. The optical density (*y*-axis) is expressed as absorbance at 660 nm (OD_{660}). Data are mean±s.d. (*n*=2) from two independent cultures. (C) CLEM of glucose-methylamine-grown cells producing DsRed–SKL and Pex32–GFP under control of the P_{AMO} promoter. The upper row shows FM images of 150-nm thick cryosections. The lower row shows an overlay of FM and EM images of the same cell section. The region of interest is indicated (dashed box). A tomogram was reconstructed and 3D rendered. Peroxisome (P), blue; ER, orange; plasma membrane, cyan. Arrows indicate the position of the center of the Pex32–GFP spot. Scale bars: FM image, 2 µm; EM images, 500 nm; 3D volume, 200 nm. A representative of four tomograms is shown. (D) FM images of glucose-grown WT (*yku80*) and *pex* mutant cells producing Pex32–GFP under control of their endogenous promoters together with the peroxisomal marker Pex14–mKate2. Scale bar: 2 µm. Representative images of three experiments are shown. (E) EM image of a KMnO4-fixed glucose-grown *pex11* mutant cell (left) and peroxisome–ER distance quantification for the *PEX11* deletion strain (right). CW, cell wall; ER, endoplasmic reticulum; P, peroxisome; M, mitochondrion. Data are mean±s.d. from two independent experiments (*n*=2 using 20 cell sections from each experiment). Scale bar: 200 nm.

pex5 atg1 control strain generally one or a few Pex32–GFP spots were present, as observed in WT cells. In *pex5 atg1* cells, small peroxisomes occur that are defective in PTS1 protein import but that harbor the complete set of peroxisomal membrane proteins (PMPs). Because PPVs in *pex3 atg1* cells and peroxisomes in *pex5 atg1* cells differ in PMP composition, we argued that those PMPs that are absent in PPVs might contribute to the accumulation of Pex32–GFP in spots. One of these PMPs is Pex11 (Knoops et al., 2014). We therefore also investigated the formation of Pex32–GFP spots in cells lacking Pex11. FM indicated that in *pex11* cells, but not in *pex25* controls, the bright Pex32–GFP spots were lost (Fig. 6D). Pex25 is also a PMP and belongs to the same protein family as Pex11. Western blot analysis showed that Pex32–GFP levels in these mutants are similar to those in WT controls, indicating that the absence of the clear Pex32–GFP spots was not due to reduced protein levels (Fig. S2). These data suggest that Pex11, but not Pex25, is specifically required for the accumulation of Pex32–GFP at peroxisome–ER contact sites.

Journal of Cell Science (2020) 133, jcs246983. doi:10.1242/jcs.246983

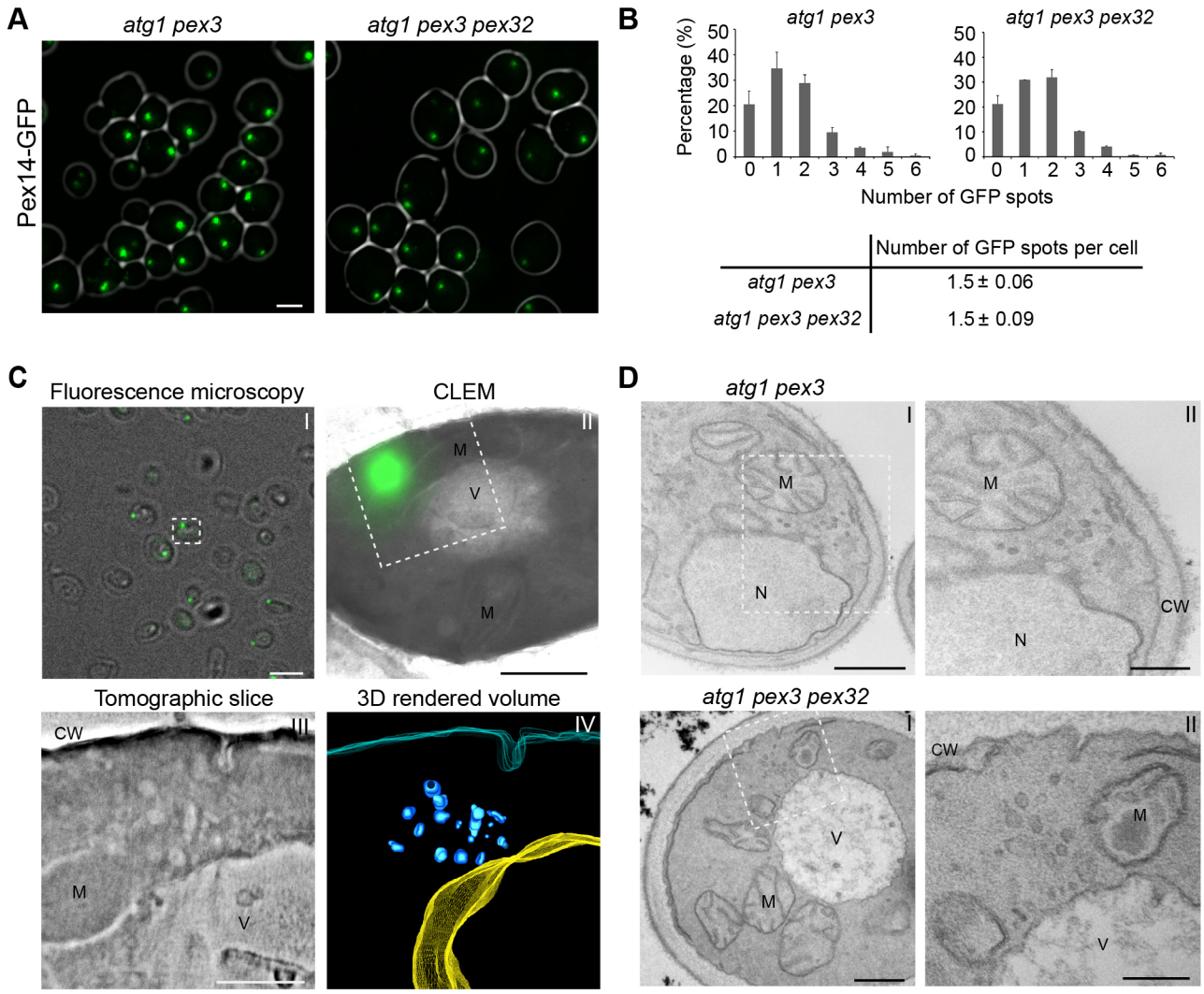

Fig. 7. Deletion of *pex32* in *pex3 atg1* cells does not result in major alterations in PPV abundance or morphology. (A) CLSM images of glycerol-methanol grown cells producing Pex14–GFP as a PPV marker. Scale bar: 2 µm. Representative images of two experiments are shown. (B) Distribution of the number of Pex14–GFP spots per cell and the average number of spots per cell. Data are mean±s.d. (*n*=2 using 280 cells from two independent experiments). (C) (I) Widefield FM image of a thick cryosection (250 nm) of *atg1 pex3 pex32* cells producing Pex14–GFP. White dashed box indicates the region shown in panel II. (II) CLEM of the region indicated in panel I, showing an overlay image of Pex14–GFP (FM) and a transmission electron micrograph of the same region. White dashed box indicates the region shown in panel III. (III) Electron tomographic slice from a tomogram recorded at the region indicated in II. (IV) 3D rendered volume of the reconstructed tomogram. PPVs (blue), vacuole (yellow) and plasma membrane (magenta) are shown. Scale bars: 2 µm, panel I; 500 nm, panel II; 200 nm, panel III. (D) EM analysis of $KMnO_4$-fixed *atg1 pex3* (upper row) and *atg1 pex3 pex32* (bottom row) cells. White dashed boxes in I indicate regions shown at higher magnification in II. Scale bars: 500 nm, panel I; 200 nm, panel II. CW, cell wall; M, mitochondrion; N, nucleus; V, vacuole.

H. polymorpha pex11 cells have several features in common with *pex32* cells. These cells show reduced growth on methanol, contain fewer, but larger, peroxisomes and show a peroxisome segregation defect (Krikken et al., 2009). This led us to examine whether *pex11* cells are also defective in peroxisome–ER contacts. Indeed, EM analysis showed that the distance between ER and peroxisomal membranes increased in *pex11* cells, as was observed for *pex32* cells (Fig. 6E). These data indicate that ER-localized Pex32 together with peroxisomal Pex11 contribute to the formation of peroxisome–ER contacts.

The absence of Pex32 does not affect PPV formation in *H. polymorpha pex3 atg1* cells

S. cerevisiae Pex30 and Pex31 are involved in the regulation of PPV formation. The absence of these proteins was reported to either stimulate (David et al., 2013; Mast et al., 2016) or delay (Joshi et al., 2016; Wang et al., 2018) PPV formation. Possibly, this relates to differences between the assays that were used to monitor PPV formation. Using Pex14–GFP as a marker for PPVs, Joshi and colleagues showed that deletion of *PEX30* or *PEX31* resulted in a significant decrease in the number of Pex14–GFP spots in *S. cerevisiae pex3 atg1* cells (Joshi et al., 2016). A similar analysis in *H. polymorpha* revealed that deletion of *PEX32* in *pex3 atg1* cells did not alter the abundance of Pex14–GFP spots (Fig. 7A,B). CLEM analysis revealed that the Pex14–GFP spots in *pex3 atg1 pex32* cells represent clusters of small vesicles (Fig. 7C). As shown in Fig. 7D, *pex32 pex3 atg1* and *pex3 atg1* control cells contain morphologically very similar clusters of vesicles. These data indicate that *H. polymorpha* Pex32 does not play an important role in the regulation of PPV formation.

Journal of Cell Science (2020) 133, jcs246983. doi:10.1242/jcs.246983

DISCUSSION

Here, we show that all four members of the *H. polymorpha* Pex23 protein family (Pex23, Pex24, Pex29 and Pex32) localize to the ER. Of these, Pex32 and Pex24 predominantly accumulated at peroxisome–ER contacts and appeared to be very important for multiple peroxisome features. Pex23 is less important for peroxisomes, and we could not detect a peroxisomal phenotype in cells lacking Pex29. Possibly, Pex23 and Pex29 play redundant roles in peroxisome biology or are involved in other functions and hence do not represent true peroxins. Pex23 also accumulated at NVJs, suggesting that Pex23 family proteins might be intrinsic contact site proteins. Initial studies revealed that in *H. polymorpha pex23* and *pex29* cells, but not in *pex24* and *pex32* cells, mitochondrial morphology and lipid body abundance is altered, suggesting that these proteins might contribute to the formation of other organelles (F.W., unpublished). Indeed, in *S. cerevisiae*, ER domains enriched in Pex30 are the sites where most nascent lipid droplets form (Joshi et al., 2018).

Analysis of an evolutionary tree revealed that HpPex23 proteins can be partitioned into two major subgroups, one containing HpPex23 and HpPex32 and the other HpPex24 and HpPex29. There is no clear correlation between subgroup and molecular function, because the strongest peroxisomal phenotypes occurred in the absence of HpPex24 and HpPex32.

The absence of *H. polymorpha* Pex24 and Pex32 resulted in the loss of peroxisome–ER contacts, accompanied by several peroxisome defects. These phenotypes could be suppressed by an artificial peroxisome ER tether protein, indicating that Pex24 and Pex32 function as contact site tethers. The peroxisomal membrane protein Pex11 also contributes to the formation of these contacts; however, we do not know whether Pex11 contributes directly or indirectly to peroxisome–ER contact formation. Interestingly, previous *P. pastoris* Pex11 pulldown experiments resulted in the identification of Pex31, a member of the *P. pastoris* Pex23 protein family (Yan et al., 2008). Moreover, David and colleagues (David et al., 2013) identified ScPex11 as a specific binding partner in ScPex29 complexes, supporting the presence of Pex11 in protein complexes at peroxisome–ER contacts. *S. cerevisiae* Pex11 is also a component of peroxisome–mitochondrion contact sites, indicating that Pex11 contributes to the formation of different membrane contacts (Mattiazzi Ušaj et al., 2015).

Our data suggest that Pex24 and Pex32 are components of tether complexes that bridge peroxisomes to the ER. However, they do not meet all three criteria suggested for bona fide tethers by Eisenberg-Bord and colleagues (Eisenberg-Bord et al., 2016). These authors proposed that tethers (1) localize or accumulate at the contact site, (2) have the structural capacity to mediate binding to two opposing membranes and (3) exert a tethering force, the existence of which may be established by demonstrating rescue using artificial tethers, among other means. Here we show that *H. polymorpha* Pex24 and Pex32 accumulate at peroxisome–ER contact sites (criterion 1) and that an artificial tether can rescue phenotypes caused by the absence of these proteins (criterion 3). Further studies are required to determine whether Pex24 and Pex32 also meet criterion 2.

The loss of peroxisome–ER contacts causes multiple phenotypes. It is not unprecedented that a contact-site-resident protein is involved in various processes. For instance the vacuolar membrane protein Vac8 functions in NVJs, vacuole fusion and inheritance in *S. cerevisiae* (Pan and Goldfarb, 1998). Moreover, the mitochondrial outer membrane protein Mdm10 is a component of ERMES and required for membrane protein insertion (Kornmann et al., 2009; Meisinger et al., 2004; Wiedemann and Pfanner, 2017).

A possible function of the Pex24-, Pex32- and Pex11-dependent peroxisome–ER contacts includes transfer of lipids from the ER to peroxisomes. Indeed, we observed reduced peroxisomal membrane surfaces in cells lacking Pex24 or Pex32. Yeast peroxisomes lack lipid biosynthetic enzymes; hence, expansion of the peroxisomal membrane relies on the supply of lipids from other sources. In *S. cerevisiae*, peroxisomal membrane lipids may originate from multiple sources, including the mitochondrion, the Golgi apparatus, the vacuole and the ER (Flis et al., 2015; Rosenberger et al., 2009). Indeed, evidence for non-vesicular lipid transport between the ER and peroxisomes in yeast has been reported previously (Raychaudhuri and Prinz, 2008).

In glucose-grown *H. polymorpha* cells the single peroxisome invariably associates with the edge of cortical ER sheets, where the ER is highly curved (Wu et al., 2018). Using CLEM, we showed that Pex32 specifically localizes to these regions. This is consistent with studies in *S. cerevisiae* that revealed that members of the Pex23 family occur in complexes with the ER-shaping reticulons, Rtn1, Rtn2, and Yop1 (David et al., 2013; Joshi et al., 2016; Mast et al., 2016). ER-shaping proteins have been implicated in lipid exchange between the ER and mitochondria in *S. cerevisiae* (Voss et al., 2012). Therefore, it is tempting to speculate that highly curved ER regions where *H. polymorpha* Pex24 and Pex32 localize function in lipid transport. Also, like *S. cerevisiae* Pex30 and Pex31, HpPex23 family proteins have a reticulon-like domain and thus might have membrane shaping properties (Joshi et al., 2016). Peroxisome–ER contact sites that contribute to phospholipid transport have also recently been identified in mammals. At these sites, the ER proteins VAPA and VAPB interact with the peroxisome membrane proteins ACBD4 and ACBD5 (Costello et al., 2017a,b; Hua et al., 2017).

Another role of peroxisome–ER contacts may be in peroxisome fission. Mitochondrion–ER contacts are important in the selection of fission sites (Friedman et al., 2011). A comparable mechanism might occur for peroxisomes. This is suggested by the presence of enlarged peroxisomes in *pex24* and *pex32* cells, similar to those observed in *pex11* cells, which are known to be defective in peroxisome fission (Williams et al., 2015). A possible alternative explanation for the enlarged peroxisomes in *H. polymorpha pex23*, *pex24* and *pex32* cells is a change in membrane lipid composition, which might interfere with peroxisome fission. Although the absence of *S. cerevisiae* Pex30 changes the ER phospholipid composition (Wang et al., 2018), it is unknown whether this peroxin influences the phospholipid content of the peroxisomal membrane.

The peroxisome–ER contacts described in this study also contribute to peroxisome positioning at the cell cortex and proper segregation of the organelles between mother cells and buds. So far, only yeast Inp1 was implicated in peroxisome retention (Fagarasanu et al., 2005; Krikken et al., 2009). Here we show that HpPex24 contributes to peroxisome retention in mother cells as well. We previously reported that *H. polymorpha pex11* cells show a peroxisome retention defect, underscoring the role of Pex11 in the formation of peroxisome–ER contacts (Krikken et al., 2009).

Proteins of the Pex23 family are implicated in the regulation of PPV formation, but are not required for their formation. Using different experimental approaches, the absence of *S. cerevisiae* Pex30 or Pex31 was shown to stimulate (David et al., 2013; Mast et al., 2016) or delay (Joshi et al., 2016; Wang et al., 2018) PPV formation. We show that in *H. polymorpha*, deletion of *PEX32* in *pex3 atg1* cells has no major effect on the abundance or morphology of PPVs, suggesting that *H. polymorpha* Pex32 does not play an important role in the regulation of PPV formation.

Journal of Cell Science (2020) 133, jcs246983. doi:10.1242/jcs.246983

In conclusion, our data indicate that Pex24 and Pex32 contribute to the tethering of peroxisomes to the ER at membrane contact sites. These contacts play multiple functions, including in peroxisome biogenesis, membrane growth, organelle proliferation and segregation.

MATERIALS AND METHODS

Strains and growth conditions

The *H. polymorpha* strains used in this study are listed in Table S2. Yeast cells were grown in batch cultures at 37°C on mineral medium (MM) (Van Dijken et al., 1976) supplemented with 0.5% glucose, 0.5% methanol or a mixture of 0.5% methanol and 0.05% glycerol as carbon sources, and 0.25% ammonium sulfate or 0.25% methylamine as nitrogen sources. When required, amino acids were added to the medium to a final concentration of 30 µg/ml. Transformants were selected on YND plates [0.67% yeast nitrogen base without amino acids (YNB; Difco, BD) and 0.5% glucose] or on YPD plates (1% yeast extract, 1% peptone and 1% glucose) containing 2% agar supplemented with 100 µg/ml zeocin (Invitrogen), 300 µg/ml hygromycin B (Invitrogen) or 100 µg/ml nourseothricin (WERNER BioAgents).

Construction of *H. polymorpha* strains

The plasmids and primers used in this study are listed in Tables S3 and S4. All plasmid integrations were performed as described previously (Faber et al., 1994). All integrations were confirmed by PCR and all deletions were confirmed by PCR and Southern blotting.

Construction of strains expressing Pex23–mGFP, Pex24–mGFP, Pex29–mGFP and Pex32–mGFP under control of endogenous promoters

A plasmid encoding Pex23–mGFP was constructed as follows: a PCR fragment encoding the C terminus of *PEX23* was obtained using primers Pex23 GFP-fw and Pex23 GFP-rev with *H. polymorpha* NCYC495 genomic DNA as a template. The obtained PCR fragment was digested with *Bgl*II and *Hin*dIII, and inserted between the *Bgl*II and *Hin*dIII sites of plasmid pHIPZ-mGFP fusinator. *Bsm*BI-linearized pHIPZ *PEX23*-mGFP was transformed into *yku80* cells, producing the strain Pex23–mGFP.

The same methods were used to construct Pex24–mGFP, Pex29–mGFP and Pex32–mGFP strains. PCR was performed on WT genomic DNA with primers Pex24 fw and Pex24 rev to amplify the C terminus of *PEX24*, primers Pex29 fw and Pex29 rev to amplify the C terminus of *PEX29*, and primers Pex32 fw and Pex32 rev to amplify the C terminus of *PEX32*. The obtained PCR fragment of *PEX24* was digested with *Bgl*II and *Hin*dIII, the PCR fragment of *PEX29* and the PCR fragment of *PEX32* were restricted by *Bam*HI and *Hin*dIII. These three digested fragments were inserted between the *Bgl*II and *Hin*dIII sites of the pHIPZ-mGFP fusinator plasmid. *Bcl*I-linearized pHIPZ *PEX24*-mGFP, *Nru*I-linearized pHIPZ *PEX29*-mGFP and *Mfe*I-linearized pHIPZ *PEX32*-mGFP were transformed into *yku80* cells separately, producing strains Pex24–mGFP, Pex29–mGFP and Pex32–mGFP. *Mun*I-linearized pHIPH *PEX14*–mKate2 was transformed into Pex23–mGFP, Pex24–mGFP, Pex29–mGFP and Pex32–mGFP cells for colocalization studies.

For the colocalization of Pex23 family proteins with the ER, *Dra*I-linearized pHIPX7 BiP_{N30}–mCherry–HDEL was integrated into Pex24–mGFP and Pex29–mGFP cells, and *Stu*I-linearized pHIPX7 BiP_{N30}–mCherry–HDEL was transformed into Pex23–mGFP cells and Pex32–mGFP cells. Plasmid pHIPX7 BiP_{N30}–mCherry–HDEL was constructed as follows: first, a PCR fragment containing *BiP* was obtained with primers KN18 and KN19 using WT genomic DNA as templates. The obtained fragment was digested with *Bam*HI and *Hin*dIII, inserted between the *Bam*HI and *Hin*dIII sites of pBlueScript II, resulting in plasmid pBS-BiP. Then a PCR fragment containing GFP–HDEL was obtained with primers KN14 and KN17 using pANL29 as template, the resulting fragment was digested with *Sal*I and *Bgl*II, and then inserted between the *Sal*I and *Bgl*II sites of pBS-BiP, resulting in pBS-BiP_{N30}–GFP–HDEL. Subsequently, pBS-BiP_{N30}–GFP–HDEL was digested with *Bam*HI/*Sal*I and inserted between the *Bam*HI/*Sal*I sites of pHIPX7 to obtain pHIPX7 BiP_{N30}–GFP–HDEL. Plasmid pHIPX7 BiP_{N30}–GFP–HDEL was digested with *Bam*HI/*Eco*RI and inserted between the *Bam*HI/*Eco*RI sites of pHIPX4, resulting in pHIPX4 BiP_{N30}–GFP–HDEL. *Not*I and *Sal*I were used to digest pHIPX4 BiP_{N30}–GFP–HDEL and inserted between the *Not*I and *Sal*I sites of pHIPZ4 DsRed–SKL to obtain plasmid pRSA017. Later, a PCR fragment was obtained using primers BIPmCh1_fw and BIPmCh1_rev on plasmid pMCE02, the resulting fragment was inserted between *Bgl*II and *Sal*I sites of pRSA017 to obtain pHIPZ4 BiP_{N30}–mCherry–HDEL. Finally, a PCR fragment was obtained by primers BIPmCh2_fw and BIPmCh1_rev using plasmid pHIPZ4 BiP_{N30}–mCherry–HDEL as a template, the resulting fragment was inserted between *Bgl*II and *Sal*I sites of pHIPX7 BiP_{N30}–GFP–HDEL, resulting in pHIPX7 BiP_{N30}–mCherry–HDEL.

Construction of strains producing Pex23–mGFP, Pex24–mGFP, Pex29–mGFP and Pex32–mGFP under control of the P_{AMO} promoter

A plasmid encoding Pex24–mGFP behind the inducible promoter amine oxidase (P_{AMO}) was constructed as follows: a PCR fragment containing *PEX24*–mGFP was obtained using primers Pex24GFP fw and Pex24GFP rev with Pex24–mGFP genomic DNA as template. This PCR product and pHIPH5 were restricted by *Sbf*I and *Bam*HI and ligated, which resulted in pHIPH5 *PEX24*–mGFP. *Pml*I-linearized pHIPH5 *PEX24*–mGFP was transformed into *yku80* or *pex32*::DsRed–SKL cells resulting in strain P_{AMO}Pex24–mGFP or strain *pex32*::DsRed–SKL::P_{AMO}Pex24–mGFP. Plasmid pHIPH5 was constructed using *Not*I- and *Sph*I-digested pHIPZ5, inserted into the *Not*I and *Sph*I sites of pHIPH4.

The plasmid pHIPH5 *PEX29*–mGFP and plasmid pHIPH5 *PEX32*–mGFP were constructed in the same way. Primers Pex29ov-fw and Pex29ov-rev were used to amplify a PCR fragment containing *PEX29*–mGFP using Pex29–mGFP genomic DNA as the template. Primers Pex32ov-fw and Pex32ov-rev were used to obtain a PCR fragment containing *PEX32*–mGFP with Pex32–mGFP genomic DNA as the template. PCR products of *PEX29*–mGFP and *PEX32*–mGFP were restricted using *Sbf*I and *Bcl*I, and inserted between the *Sbf*I and *Bcl*I sites of pHIPH5 *PEX24*–mGFP, respectively, to make plasmid pHIPH5 *PEX29*–mGFP and pHIPH5 *PEX32*–mGFP. *Nar*I-linearized pHIPH5 *PEX29*–mGFP and pHIPH5 *PEX32*–mGFP were integrated into *yku80* or *pex32*::DsRed–SKL cells separately to overproduce Pex29–mGFP and Pex32–mGFP.

The plasmid of pHIPH5 *PEX23*–mGFP was constructed in two steps. First, a PCR fragment containing partial (no start codon) *PEX23*–mGFP was obtained using primers Pex23ov-fw and Pex23ov-rev with Pex23–mGFP genomic DNA as a template. The PCR product and pHIPH5 *PEX24*–mGFP were restricted using *Sbf*I and *Bam*HI and ligated to produce pHIPH5 *PEX23p*–mGFP. Next, a PCR using primers Pex23ov2-fw and Pex23ov2-rev was performed to obtain the left partial (with start codon) *PEX23*–mGFP fragment using plasmid pHIPH5 *PEX24*–mGFP as template. The PCR product and pHIPH5 *PEX23p*–mGFP were restricted using *Not*I and *Bam*HI, then ligated to produce pHIPH5 *PEX23*–mGFP. *Nar*I-linearized pHIPH5 *PEX23*–mGFP was transformed into *yku80* or *pex32*::DsRed–SKL cells to overproduce Pex23–mGFP.

*Eco*RI-linearized pHIPN18 DsRed–SKL was integrated into *yku80*, P_{AMO}Pex23–mGFP, P_{AMO}Pex24–mGFP, P_{AMO}Pex29–mGFP and P_{AMO}Pex32–mGFP cells. A plasmid encoding pHIPN18 DsRed–SKL was constructed as follows: a vector fragment was obtained by *Hin*dIII and *Sal*I digestion of pHIPN18 GFP–SKL, whereas the DsRed–SKL insertion fragment was obtained by *Hin*dIII and *Sal*I digestion of pHIPZ4 DsRed–SKL; ligation resulted in the plasmid pHIPN18 DsRed–SKL. Plasmid pHIPN18 GFP–SKL was constructed by inserting *Not*I- and *Xba*I-digested pAMK94 into the *Not*I and *Xba*I sites of pHIPN4. Plasmid pAMK94 was constructed as follows: a PCR fragment containing *ADH1* was amplified using primers ADH1 fw and ADH1 rev with WT genomic DNA as template. *Not*I- and *Hin*dIII-digested PCR product was then inserted into *Not*I and *Hin*dIII sites of pHIPZ4 eGFP–SKL.

*Mun*I-linearized pHIPN *VAC8*–mKate2 was integrated into Pex23–mGFP and P_{AMO}Pex24–GFP cells to produce Vac8–mKate2. Plasmid pHIPN *VAC8*–mKate2 was constructed by fragment ligation from *Hin*dIII/*Sal*I digested plasmid pHIPZ *VAC8*–mKate2 and *Hin*dIII/*Sal*I digested plasmid pHIPN *PEX14*–mCherry. Plasmid pHIPZ *VAC8*–GFP and plasmid pHIPZ *PEX14*–mKate2 were digested with *Hin*dIII and *Bgl*II and ligated to obtain

Journal of Cell Science (2020) 133, jcs246983. doi:10.1242/jcs.246983

plasmid pHIPZ *VAC8*–mKate2. Plasmid pHIPZ *VAC8*–GFP was constructed by amplification of the *VAC8* gene, lacking the stop codon, using primers Vac8_BglII R and Vac8_F and genomic DNA as template. The resulting PCR product was digested with *Hin*dIII and *Bgl*II, and ligated between the *Hin*dIII and *Bgl*II sites of the pHIPZ–mGFP fusinator plasmid.

Construction of *pex23*, *pex24*, *pex29* and *pex32* deletion strains

The *pex23* deletion strain was constructed by replacing the *PEX23* region with the zeocin resistance gene as follows: first, a PCR fragment containing the zeocin resistance gene and 50 bp of the *PEX23* flanking regions was amplified with primers PEX23-Fw and PEX23-Rev using plasmid pENTR221-zeocin as template. The resulting *PEX23* deletion cassette was transformed into *yku80* cells to obtain strain *pex23*. *PEX24*, *PEX29* and *PEX32* were also replaced by the zeocin resistance gene in the same way. Primers for the *PEX24* deletion cassette were PEX24-Fw and PEX24-Rev, primers for the *PEX29* deletion cassette were dPEX29-F and dPEX29-R, and primers for the *PEX32* deletion cassette were dPEX32-F and dPEX32-R. These three deletion cassettes were transformed into y*ku80* cells, producing *pex24*, *pex29* and *pex32*, respectively.

For expression of GFP–SKL in WT (*yku80*) and deletion mutant strains, *Stu*I-linearized pHIPN7 GFP–SKL was transformed into *pex23* and *pex24* mutant cells, and *Ahd*I-linearized pFEM35 was transformed into *yku80*, *pex29* and *pex32* mutant cells.

The *Mun*I-linearized pHIPN *PMP47*–mGFP plasmid was transformed into *pex23*, *pex24*, *pex29* and *pex32* cells. Plasmid pHIPN *PMP47*–mGFP was constructed as follows: a PCR fragment encoding the nourseothricin resistance gene was obtained with primers Nat-fwd and Nat-rev using plasmid pHIPN4 as a template. The obtained PCR fragment was digested with *Not*I and *Xho*I and inserted between the *Not*I and *Xho*I sites of pMCE7, resulting in plasmid pHIPN *PMP47*–mGFP.

The *Dra*I-linearized pAMK15 was transformed into *pex32* cells to obtain a strain producing DsRed–SKL.

Construction of *pex23* family mutants with or without an artificial ERPER tether

To introduce an artificial peroxisome–ER tether, two plasmids, pARM115 (pHIPH18 *PEX14*) and pARM118 (pHIPH18 *PEX14*–2HA–*UBC6*), were constructed as follows. A PCR fragment containing *PEX14* was amplified with primers Pex14-HindIII-fw and Pex14-PspXI-rev using WT genomic DNA as a template. The PCR fragment was digested with *Hin*dIII and *Psp*XI, then inserted between the *Hin*dIII and *Sal*I sites of pAMK94 to get plasmid pHIPZ18 *PEX14*. A *Not*I/*Bpi*I digested fragment from plasmid pHIPZ18 *PEX14* and a *Not*I/*Bpi*I digested fragment from plasmid pHIPH4 were ligated, resulting in plasmid pARM115. The *Age*I-linearized pARM115 was transformed into *yku80*::GFP–SKL and *pex32*::GFP–SKL cells to produce P_{ADH1}Pex14 (Pex14++). A PCR fragment containing *PEX14*–2×HA was amplified by primers HindIII-Pex14 and Pex14-HA-HA. A fragment containing 2×HA–*UBC6* was amplified with primers HAHA-Ubc6 and Ubc6-PspXI using WT genomic DNA as template. The obtained PCR fragments were purified and used as templates together with primers HindIII-Pex14 and Ubc6-PspXI in a second PCR reaction. The obtained overlap PCR fragment was digested with *Hin*dIII and *Psp*XI, and inserted between the *Hin*dIII and *Sal*I sites of pAMK94, resulting in plasmid pARM053 (pHIPZ18 *PEX14*–2HA–*UBC6*). A *Not*I/*Bpi*I digested fragment from plasmid pAMK053 and a *Not*I/*Bpi*I digested fragment from plasmid pHIPH4 were ligated, resulting in plasmid pARM118. Then the *Age*I-linearized pARM118 was transformed into *yku80*::GFP–SKL, *yku80*::Pmp47–GFP, *pex23*::GFP–SKL, *pex24*::GFP–SKL, *pex24*::Pmp47–GFP, *pex29*::GFP–SKL, *pex32*::GFP–SKL and *pex32*::Pmp47–GFP cells, to produce P_{ADH1}Pex14–2HA–Ubc6 (ERPER)-expressing strains.

Expression of Pex32–mGFP in different *pex* mutant cells

The *Bgl*II-linearized pHIPZ *PEX32*–mGFP was transformed into *pex3 atg1*::Pex14–mCherry, *pex5 atg1*::Pex14–mCherry, *pex11* and *pex25* cells, to produce Pex32–mGFP-expressing stains. *Blp*I-linearized pARM014 (pHIPX7 *PEX14*–mCherry) was transformed into *pex5 atg1* cells, which resulted in *pex5 atg1*::Pex14–mCherry. Plasmid pARM014 was constructed through the following steps: first, a PCR fragment containing Pex14–mCherry was amplified with primers PRARM001 and PRARM002 using pSEM01 as a template. The obtained PCR fragment was digested with *Not*I and *Hin*dIII, and inserted between the *Not*I and *Hin*dIII sites of plasmid pHIPX7, resulting in plasmid pARM014. An *ATG1* deletion cassette was amplified by PCR with primers pDEL-ATG1-fwd and pDEL-ATG1-rev using plasmid pARM011 as template. Then the PCR product was integrated into *pex5* cells to make the *pex5 atg1* mutant.

Two plasmids allowing disruption of *H. polymorpha PEX25* were constructed using Multisite Gateway technology, as follows. First, the 5′ and 3′ flanking regions of the *PEX25* gene were amplified by PCR with primers RSAPex25-1 and RSAPex25-2, and RSAPex25-3 and RSAPex25-4, respectively, using *H. polymorpha* NCYC495 genomic DNA as a template. The resulting fragments were then recombined in donor vectors pDONR P4-P1R and pDONR P2R-P3, resulting in plasmids pENTR-PEX25 5′ and pENTR-PEX25 3′, respectively. Then, PCR amplification was performed using primers attB1-Ptef1-forward and attB2-Ttef1-reverse using pHIPN4 as the template. The resulting PCR fragment was recombined into vector pDONR-221, yielding entry vector pENTR-221-NAT. Recombination of the entry vectors pENTR-PEX25 5′, pENTR-221-NAT, and pENTR-PEX25 3′, and the destination vector pDEST-R4-R3, resulted in pRSA018. Then, a *PEX25* disruption cassette containing nourseothricin resistance gene was amplified with primers RSAPex25-5 and RSAPex25-6 using pRSA018 as a template. To create the *pex25* mutant, the *PEX25* disruption cassette was transformed into *yku80* cells. *Blp*I-linearized pHIPH *PEX14*–mCherry was integrated into *pex11*::Pex32–mGFP or *pex25*::Pex32–mGFP to produce Pex14–mCherry.

Construction of *pex32 inp1* double and *pex3 atg1 pex32* triple deletion strains

To construct the *pex32 inp1* mutant, a PCR fragment containing an *INP1* deletion cassette was amplified with primers dInp1FW-F and dInp1-REV using plasmid pHIPH5 as a template. The resulting *INP1* deletion cassette was transformed into *pex32* cells for double deletion of *pex32 inp1*. The *Ahd*I-linearized pFEM35 was transformed into *pex32 inp1* to produce GFP–SKL-expressing cells.

To construct the *pex3 atg1 pex32* strain, a PCR fragment containing the *PEX32* deletion cassette was amplified with primers dPex32-F and dPex32-R using *pex32* genomic DNA as a template. The resulting *PEX32* deletion cassette was transformed into *pex3 atg1* cells to get a triple mutant of *pex3 atg1 pex32*. *Xho*I-linearized pHIPN *PEX14*–mGFP plasmid was integrated into *pex3 atg1 pex32* cells.

The plasmid encoding pHIPN *PEX14*–mGFP was constructed as follows: a PCR fragment containing the nourseothricin resistance gene was obtained using primers Nat fw and Nat rev with plasmid pHIPN4 as a template. The PCR product and pSNA12 were digested with *Nsi*I and *Not*I, then ligated to produce pHIPN *PEX14*–mGFP.

Molecular and biochemical techniques

DNA restriction enzymes were used as recommended by the suppliers (Thermo Fisher Scientific or New England Biolabs). PCR for cloning was carried out using Phusion High-Fidelity DNA Polymerase (Thermo Fisher Scientific). An initial selection of positive transformants by colony PCR was carried out using Phire polymerase (Thermo Fisher Scientific). For DNA and amino acid sequence analysis, the Clone Manager 5 program (Scientific and Educational Software, Durham, NC) was used.

For western blot analysis, total cell extracts were prepared as described previously (Baerends et al., 2000). Samples in Fig. 2E were denatured in urea loading buffer (25mM Tris-HCl pH 6.8, 0.8% SDS, 3.5% glycerol, 4 M urea, 2% β-mercaptoethanol and 0.008% Bromophenol Blue). Blots were decorated using anti-GFP antibodies (sc-996, Santa Cruz Biotech; 1:2000 dilution), anti-pyruvate carboxylase-1 (Pyc1) antibodies (Ozimek et al., 2007, 1:10,000 dilution) or anti-Pex14 antibodies (Komori et al., 1997, 1:10,000 dilution). Secondary goat anti-rabbit (31460) or goat anti-mouse (31430) antibodies conjugated to horseradish peroxidase (HRP) (Thermo Scientific; 1:5000 dilution) were used for detection. Blots were scanned by using a densitometer (GS-710; Bio-Rad Laboratories).

Fluorescence microscopy

Widefield FM images of living cells and of cryosections for CLEM were captured at room temperature using a 100×1.30 NA objective (Carl Zeiss, Oberkochen, Germany). Images were obtained from the cells in growth medium using a fluorescence microscope (Axioscope A1; Carl Zeiss), Micro-Manager 1.4 software and a digital camera (Coolsnap HQ^2; Photometrics). GFP fluorescence was visualized using a 470/40 nm band-pass excitation filter, a 495 nm dichromatic mirror, and a 525/50 nm band-pass emission filter. DsRed fluorescence was visualized using a 546/12 nm band-pass excitation filter, a 560 nm dichromatic mirror, and a 575–640 nm band-pass emission filter. mCherry and mKate2 fluorescence were visualized using a 587/25 nm band-pass excitation filter, a 605 nm dichromatic mirror, and a 670/70 nm band-pass emission filter.

Confocal images were captured with an LSM800 Airyscan confocal microscope (Carl Zeiss) using Zen 2.3 software (Carl Zeiss) and a 100×/1.40 plan apochromat objective and GaAsP detectors. For quantitative analysis of peroxisomes or Pex14–mGFP fluorescent spots, *z*-stacks were made of randomly chosen fields.

Image analysis was performed using ImageJ, all brightfield images have been adjusted to only show cell outlines. Figures were prepared using Adobe Illustrator software.

Electron microscopy

For morphological analysis, cells were fixed in 1.5% potassium permanganate, post-stained with 0.5% uranyl acetate and embedded in Epon [a mixture of Glycid ether (51.5% w/v; Serva, 151414), Methylnadic anhydride (47.3% w/v; Serva, 140573) and 2,4,6-Tris (dimethylaminomethyl)phenol (1.2% w/v; Santa Cruz, F0112)]. Image analysis and distance measurements are performed using ImageJ. For the quantification of the ER, the total length of the plasma membrane and the peripheral ER was measured from cell sections, and from this the percentage of the cortex covered by the ER was calculated. Correlative light and electron microscopy (CLEM) was performed using cryosections, as described previously (Knoops et al., 2015). After fluorescence imaging, the grid was post-stained and embedded in a mixture of 0.5% uranyl acetate and 0.5% methylcellulose. Acquisition of the double-tilt tomography series was performed manually in a CM12 TEM (Philips) running at 100 kV, and included a tilt range of 40° to −40° with 2.5° increments. To construct the CLEM images, pictures taken with FM and EM were aligned using the eC-CLEM plugin in Icy (Paul-Gilloteaux et al., 2017) (http://icy.bioimageanalysis.org). Reconstruction of the tomograms was performed using the IMOD software package (https://bio3d.colorado.edu/imod/).

Immuno-EM was performed as described previously (Thomas et al., 2018). Labeling of HA was performed using monoclonal antibodies (Sigma-Aldrich H9658; 1:100 dilution) followed by goat anti-mouse antibodies conjugated to 6 nm gold (Aurion, The Netherlands; 1:20 dilution).

In silico analyses

Homologous sequences were detected using BLASTP with an E-value threshold of 1e-5 (Altschul et al., 1990). Linear and secondary structure predictions were realized using Foundation (Bordin et al., 2018).

Phylogenetic tree

The multiple sequence alignment used as input was created using ClustalOmega (Sievers et al., 2011), using default parameters, and manually curated in Jalview (Waterhouse et al., 2009). The tree was generated using PhyML 3.1 (Guindon et al., 2010) using the LG matrix, 100 bootstraps, tree and leaves refinement, SPR moves, and amino acids substitution rates determined empirically.

Peroxisome membrane surface area calculation

For peroxisome membrane surface area calculation: the average peroxisome volume (V) and average peroxisome number per cell (N) were determined using a plugin for ImageJ (Thomas et al., 2015) from two independent experiments (2×300 cells were counted). The formula $V=(4/3)\pi r^3$ was used to calculate peroxisome radius (r), and formula $S=4\pi r^2$ was used to calculate the average peroxisome surface area (S). The average peroxisome number per cell N multiplied with S is the peroxisome membrane surface area per cell.

Quantification of the distance between GFP spots and the cell cortex

For the calculation of the distance between GFP–SKL spots and the cell cortex, cells containing GFP spots were selected and processed using ImageJ. Subsequently, the distance between the middle of the GFP spot and the cell outline was measured. For cells containing two or more GFP spots, only the spot closest to the cell outline was used.

Peroxisome inheritance quantification

Peroxisome inheritance quantification was performed using a method published previously (Krikken et al., 2009).

Acknowledgements

We thank Benjan Karnebeek, Malgorzata Krygowska and Kim van Maldegem for assistance in strain construction and Tim Levine (University College London, UK) for advice in protein sequence analysis.

Competing interests

The authors declare no competing or financial interests.

Author contributions

Conceptualization: F.W., R.d.B., A.M.K., A.A., I.J.v.d.K.; Methodology: F.W., R.d.B., A.M.K., A.A., I.J.v.d.K.; Validation: F.W., R.d.B., I.J.v.d.K.; Formal analysis: F.W., R.d.B., A.M.K., A.A., N.B., D.P.D.; Investigation: F.W., R.d.B., A.M.K., A.A., N.B., D.P.D.; Writing - original draft: F.W., I.J.v.d.K.; Writing - review & editing: F.W., R.d.B., A.M.K., A.A., N.B., D.P.D., I.J.v.d.K.; Supervision: I.J.v.d.K.; Project administration: I.J.v.d.K.; Funding acquisition: I.J.v.d.K.

Funding

This work was supported by a grant from the FP7 People: Marie-Curie Actions Initial Training Networks (ITN) program PerFuMe (Grant Agreement Number 316723) to N.B., D.P.D. and I.J.v.d.K., from the China Scholarship Council (CSC) to F.W., and from the Nederlandse Organisatie voor Wetenschappelijk Onderzoek/Chemical Sciences (NWO/CW) to A.A. (711.012.002).

Supplementary information

Supplementary information available online at
https://jcs.biologists.org/lookup/doi/10.1242/jcs.246983.supplemental

Peer review history

The peer review history is available online at
https://jcs.biologists.org/lookup/doi/10.1242/jcs.246983.reviewer-comments.pdf

References

Altschul, S. F., Gish, W., Miller, W., Myers, E. W. and Lipman, D. J. (1990). Basic local alignment search tool. *J. Mol. Biol.* **215**, 403-410. doi:10.1016/S0022-2836(05)80360-2

Baerends, R. J. S., Faber, K. N., Kram, A. M., Kiel, J. A. K. W., van der Klei, I. J. and Veenhuis, M. (2000). A stretch of positively charged amino acids at the N terminus of Hansenula polymorpha Pex3p is involved in incorporation of the protein into the peroxisomal membrane. *J. Biol. Chem.* **275**, 9986-9995. doi:10.1074/jbc.275.14.9986

Bansal, D. and Campbell, K. P. (2004). Dysferlin and the plasma membrane repair in muscular dystrophy. *Trends Cell Biol.* **14**, 206-213. doi:10.1016/j.tcb.2004.03.001

Bansal, D., Miyake, K., Vogel, S. S., Groh, S., Chen, C.-C., Williamson, R., McNeil, P. L. and Campbell, K. P. (2003). Defective membrane repair in dysferlin-deficient muscular dystrophy. *Nature* **423**, 168-172. doi:10.1038/nature01573

Bordin, N., González-Sánchez, J. C. and Devos, D. P. (2018). PVCbase: an integrated web resource for the PVC bacterial proteomes. *Database* **2018**, 1-10. doi:10.1093/database/bay042

Brown, T. W., Titorenko, V. I. and Rachubinski, R. A. (2000). Mutants of the *Yarrowia lipolytica PEX23* gene encoding an integral peroxisomal membrane peroxin mislocalize matrix proteins and accumulate vesicles containing peroxisomal matrix and membrane proteins. *Mol. Biol. Cell* **11**, 141-152. doi:10.1091/mbc.11.1.141

Cepińska, M. N., Veenhuis, M., van der Klei, I. J. and Nagotu, S. (2011). Peroxisome Fission is Associated with Reorganization of Specific Membrane Proteins. *Traffic* **12**, 925-937. doi:10.1111/j.1600-0854.2011.01198.x

Costello, J. L., Castro, I. G., Hacker, C., Schrader, T. A., Metz, J., Zeuschner, D., Azadi, A. S., Godinho, L. F., Costina, V., Findeisen, P. et al. (2017a). ACBD5

and VAPB mediate membrane associations between peroxisomes and the ER. *J. Cell Biol.* **216**, 331-342. doi:10.1083/jcb.201607055

Costello, J. L., Castro, I. G., Schrader, T. A., Islinger, M. and Schrader, M. (2017b). Peroxisomal ACBD4 interacts with VAPB and promotes ER-peroxisome associations. *Cell Cycle* **16**, 1039-1045. doi:10.1080/15384101.2017.1314422

David, C., Koch, J., Oeljeklaus, S., Laernsack, A., Melchior, S., Wiese, S., Schummer, A., Erdmann, R., Warscheid, B. and Brocard, C. (2013). A combined approach of quantitative interaction proteomics and live-cell imaging reveals a regulatory role for Endoplasmic Reticulum (ER) reticulon homology proteins in peroxisome biogenesis. *Mol. Cell. Proteomics* **12**, 2408-2425. doi:10.1074/mcp.M112.017830

Distel, B., Erdmann, R., Gould, S. J., Blobel, G., Crane, D. I., Cregg, J. M., Dodt, G., Fujiki, Y., Goodman, J. M., Just, W. W. et al. (1996). A unified nomenclature for peroxisome biogenesis factors. *J. Cell Biol.* **135**, 1-3. doi:10.1083/jcb.135.1.1

Eisenberg-Bord, M., Shai, N., Schuldiner, M. and Bohnert, M. (2016). A tether is a tether is a tether: tethering at membrane contact sites. *Dev. Cell* **39**, 395-409. doi:10.1016/j.devcel.2016.10.022

Faber, K. N., Haima, P., Harder, W., Veenhuis, M. and Ab, G. (1994). Highly-efficient electrotransformation of the yeast Hansenula polymorpha. *Curr. Genet.* **25**, 305-310. doi:10.1007/BF00351482

Fagarasanu, M., Fagarasanu, A., Tam, Y. Y. C., Aitchison, J. D. and Rachubinski, R. A. (2005). Inp1p is a peroxisomal membrane protein required for peroxisome inheritance in Saccharomyces cerevisiae. *J. Cell Biol.* **169**, 765-775. doi:10.1083/jcb.200503083

Flis, V. V., Fankl, A., Ramprecht, C., Zellnig, G., Leitner, E., Hermetter, A. and Daum, G. (2015). Phosphatidylcholine supply to peroxisomes of the yeast Saccharomyces cerevisiae. *PLoS ONE* **10**, 1-19. doi:10.1371/journal.pone.0140080

Friedman, J. R., Lackner, L. L., West, M., DiBenedetto, J. R., Nunnari, J. and Voeltz, G. K. (2011). ER tubules mark sites of mitochondrial division. *Science* **334**, 358-362. doi:10.1126/science.1207385

Guindon, S., Dufayard, J.-F., Lefort, V., Anisimova, M., Hordijk, W. and Gascuel, O. (2010). New algorithms and methods to estimate maximum-likelihood phylogenies: assessing the performance of PhyML 3.0. *Syst. Biol.* **59**, 307-321. doi:10.1093/sysbio/syq010

Hua, R., Cheng, D., Coyaud, É., Freeman, S., Di Pietro, E., Wang, Y., Vissa, A., Yip, C. M., Fairn, G. D., Braverman, N. et al. (2017). VAPs and ACBD5 tether peroxisomes to the ER for peroxisome maintenance and lipid homeostasis. *J. Cell Biol.* **216**, 367-377. doi:10.1083/jcb.201608128

Joshi, A. S., Huang, X., Choudhary, V., Levine, T. P., Hu, J. and Prinz, W. A. (2016). A family of membrane-shaping proteins at ER subdomains regulates pre-peroxisomal vesicle biogenesis. *J. Cell Biol.* **215**, 515-529. doi:10.1083/jcb.201602064

Joshi, A. S., Nebenfuehr, B., Choudhary, V., Satpute-Krishnan, P., Levine, T. P., Golden, A. and Prinz, W. A. (2018). Lipid droplet and peroxisome biogenesis occur at the same ER subdomains. *Nat. Commun.* **9**, 2940. doi:10.1038/s41467-018-05277-3

Kiel, J. A. K. W., Veenhuis, M. and van der Klei, I. J. (2006). PEX genes in fungal genomes: common, rare or redundant. *Traffic* **7**, 1291-1303. doi:10.1111/j.1600-0854.2006.00479.x

Knoblach, B., Sun, X., Coquelle, N., Fagarasanu, A., Poirier, R. L. and Rachubinski, R. A. (2013a). An ER-peroxisome tether exerts peroxisome population control in yeast. *EMBO J.* **32**, 2439-2453. doi:10.1038/emboj.2013.170

Knoops, K., Manivannan, S., Cepińska, M. N., Krikken, A. M., Kram, A. M., Veenhuis, M. and van der Klei, I. J. (2014). Preperoxisomal vesicles can form in the absence of Pex3. *J. Cell Biol.* **204**, 659-668. doi:10.1083/jcb.201310148

Knoops, K., de Boer, R., Kram, A. and Van Der Klei, I. J. (2015). Yeast pex1 cells contain peroxisomal ghosts that import matrix proteins upon reintroduction of Pex1. *J. Cell Biol.* **211**, 955-962. doi:10.1083/jcb.201506059

Komori, M., Rasmussen, S. W., Kiel, J. A. K. W., Baerends, R. J. S., Cregg, J. M., Van Der Klei, I. J. and Veenhuis, M. (1997). The Hansenula polymorpha PEX14 gene encodes a novel peroxisomal membrane protein essential for peroxisome biogenesis. *EMBO J.* **16**, 44-53. doi:10.1093/emboj/16.1.44

Kornmann, B., Currie, E., Collins, S. R., Schuldiner, M., Nunnari, J., Weissman, J. S. and Walter, P. (2009). An ER-mitochondria tethering complex revealed by a synthetic biology screen. *Science* **325**, 477-481. doi:10.1126/science.1175088

Krikken, A. M., Veenhuis, M. and van der Klei, I. J. (2009). Hansenula polymorpha pex11 cells are affected in peroxisome retention. *FEBS J.* **276**, 1429-1439. doi:10.1111/j.1742-4658.2009.06883.x

Lek, A., Evesson, F. J., Sutton, R. B., North, K. N. and Cooper, S. T. (2011). Ferlins: regulators of vesicle fusion for auditory neurotransmission, receptor trafficking and membrane repair. *Traffic* **13**, 185-194. doi:10.1111/j.1600-0854.2011.01267.x

Lv, X., Liu, J., Qin, Y., Liu, Y., Jin, M., Dai, J., Chua, B. T., Yang, H. and Li, P. (2019). Identification of gene products that control lipid droplet size in yeast using a high-throughput quantitative image analysis. *Biochim. Biophys. Acta Mol. Cell Biol. Lipids* **1864**, 113-127. doi:10.1016/j.bbalip.2018.11.001

Ma, W. and Goldberg, J. (2013). Rules for the recognition of dilysine retrieval motifs by coatomer. *EMBO J.* **32**, 926-937. doi:10.1038/emboj.2013.41

Mast, F. D., Jamakhandi, A., Saleem, R. A., Dilworth, D. J., Rogers, R. S., Rachubinski, R. A. and Aitchison, J. D. (2016). Peroxins Pex30 and Pex29 dynamically associate with reticulons to regulate peroxisome biogenesis from the endoplasmic reticulum. *J. Biol. Chem.* **291**, 15408-15427. doi:10.1074/jbc.M116.728154

Mattiazzi Ušaj, M., Brložnik, M., Kaferle, P., Žitnik, M., Wolinski, H., Leitner, F., Kohlwein, S. D., Zupan, B. and Petrovič, U. (2015). Genome-wide localization study of yeast pex11 identifies peroxisome-mitochondria interactions through the ERMES complex. *J. Mol. Biol.* **427**, 2072-2087. doi:10.1016/j.jmb.2015.03.004

Meisinger, C., Rissler, M., Chacinska, A., Szklarz, L. K. S., Milenkovic, D., Kozjak, V., Schönfisch, B., Lohaus, C., Meyer, H. E., Yaffe, M. P. et al. (2004). The mitochondrial morphology protein mdm10 functions in assembly of the preprotein translocase of the outer membrane. *Dev. Cell* **7**, 61-71. doi:10.1016/j.devcel.2004.06.003

Ozimek, P. Z., Klompmaker, S. H., Visser, N., Veenhuis, M. and van der Klei, I. J. (2007). The transcarboxylase domain of pyruvate carboxylase is essential for assembly of the peroxisomal flavoenzyme alcohol oxidase. *FEMS Yeast Res.* **7**, 1082-1092. doi:10.1111/j.1567-1364.2007.00214.x

Pan, X. and Goldfarb, D. S. (1998). YEB3/VAC8 encodes a myristylated armadillo protein of the Saccharomyces cerevisiae vacuolar membrane that functions in vacuole fusion and inheritance. *J. Cell Sci.* **111**, 2137-2147.

Paul-Gilloteaux, P., Heiligenstein, X., Belle, M., Domart, M.-C., Larijani, B., Collinson, L., Raposo, G. and Salamero, J. (2017). Erratum: Corrigendum: eC-CLEM: flexible multidimensional registration software for correlative microscopies. *Nat. Methods* **14**, 323-323. doi:10.1038/nmeth0317-323a

Raychaudhuri, S. and Prinz, W. A. (2008). Nonvesicular phospholipid transfer between peroxisomes and the endoplasmic reticulum. *Proc. Natl. Acad. Sci. USA* **105**, 15785-15790. doi:10.1073/pnas.0808321105

Rosenberger, S., Connerth, M., Zellnig, G. and Daum, G. (2009). Phosphatidylethanolamine synthesized by three different pathways is supplied to peroxisomes of the yeast Saccharomyces cerevisiae. *Biochim. Biophys. Acta* **1791**, 379-387. doi:10.1016/j.bbalip.2009.01.015

Sievers, F., Wilm, A., Dineen, D., Gibson, T. J., Karplus, K., Li, W., Lopez, R., McWilliam, H., Remmert, M., Söding, J. et al., (2011). Fast, scalable generation of high-quality protein multiple sequence alignments using Clustal Omega. *Mol. Syst. Biol.* **7**, 539. doi:10.1038/msb.2011.75

Tam, Y. Y. C. and Rachubinski, R. A. (2002). Yarrowia lipolytica cells mutant for the PEX24 gene encoding a peroxisomal membrane peroxin mislocalize peroxisomal proteins and accumulate membrane structures containing both peroxisomal matrix and membrane proteins. *Mol. Biol. Cell* **13**, 2681-2691. doi:10.1091/mbc.e02-02-0117

Thomas, A. S., Krikken, A. M., van der Klei, I. J. and Williams, C. P. (2015). Phosphorylation of Pex11p does not regulate peroxisomal fission in the yeast Hansenula polymorpha. *Sci. Rep.* **5**, 1733. doi:10.1038/srep11493

Thomas, A. S., Krikken, A. M., de Boer, R. and Williams, C. (2018). Hansenula polymorpha Aat2p is targeted to peroxisomes via a novel Pex20p-dependent pathway. *FEBS Lett.* **592**, 2466-2475. doi:10.1002/1873-3468.13168

van der Klei, I. J., Yurimoto, H., Sakai, Y. and Veenhuis, M. (2006). The significance of peroxisomes in methanol metabolism in methylotrophic yeast. *Biochim. Biophys. Acta* **1763**, 1453-1462. doi:10.1016/j.bbamcr.2006.07.016

Van Dijken, L. P., Otto, R. and Harder, W. (1976). Growth of Hansenula polymorpha in a methanol-limited chemostat. *Arch. Microbiol.* **111**, 137-144. doi:10.1007/BF00446560

Vizeacoumar, F. J., Torres-Guzman, J. C., Tam, Y. Y. C., Aitchison, J. D. and Rachubinski, R. A. (2003). YHR150w and YDR479c encode peroxisomal integral membrane proteins involved in the regulation of peroxisome number, size, and distribution in Saccharomyces cerevisiae. *J. Cell Biol.* **161**, 321-332. doi:10.1083/jcb.200210130

Vizeacoumar, F. J., Torres-Guzman, J. C., Bouard, D., Aitchison, J. D. and Rachubinski, R. A. (2004). Pex30p, Pex31p, and Pex32p form a family of peroxisomal integral membrane proteins regulating peroxisome size and number in Saccharomyces cerevisiae. *Mol. Biol. Cell* **15**, 665-677. doi:10.1091/mbc.e03-09-0681

Voss, C., Lahiri, S., Young, B. P., Loewen, C. J. and Prinz, W. A. (2012). ER-shaping proteins facilitate lipid exchange between the ER and mitochondria in S. cerevisiae. *J. Cell Sci.* **125**, 4791-4799. doi:10.1242/jcs.105635

Wang, S., Idrissi, F.-Z., Hermansson, M., Grippa, A., Ejsing, C. S. and Carvalho, P. (2018). Seipin and the membrane-shaping protein Pex30 cooperate in organelle budding from the endoplasmic reticulum. *Nat. Commun.* **9**, 1-12. doi:10.1038/s41467-018-05278-2

Waterhouse, A. M., Procter, J. B., Martin, D. M. A., Clamp, M. and Barton, G. J. (2009). Jalview Version 2-A multiple sequence alignment editor and analysis workbench. *Bioinformatics* **25**, 1189-1191. doi:10.1093/bioinformatics/btp033

Wiedemann, N. and Pfanner, N. (2017). Mitochondrial machineries for protein import and assembly. *Annu. Rev. Biochem.* **86**, 685-714. doi:10.1146/annurev-biochem-060815-014352

Williams, C., Opalinski, L., Landgraf, C., Costello, J., Schrader, M., Krikken, A. M., Knoops, K., Kram, A. M., Volkmer, R. and van der Klei, I. J. (2015). The membrane remodeling protein Pex11p activates the GTPase Dnm1p during

peroxisomal fission. *Proc. Natl. Acad. Sci. USA* **112**, 6377-6382. doi:10.1073/pnas.1418736112

Wu, H. (2020). Pex3-mediated peroxisomal membrane contact sites in yeast. *PhD thesis*, University of Groningen, Groningen, the Netherlands. doi:10.33612/diss.113450193

Wu, H., de Boer, R., Krikken, A. M., Akşit, A., Yuan, W. and van der Klei, I. J. (2018). Peroxisome development in yeast is associated with the formation of Pex3-dependent peroxisome-vacuole contact sites. *Biochim. Biophys. Acta Mol. Cell Res.* **1866**, 349-359. doi:10.1016/j.bbamcr.2018.08.021

Yan, M., Rachubinski, D. A., Joshi, S., Rachubinski, R. A. and Subramani, S. (2008). Dysferlin domain-containing proteins, Pex30p and Pex31p, localized to two compartments, control the number and size of Oleate-induced peroxisomes in Pichia pastoris. *Mol. Biol. Cell* **19**, 885-898. doi:10.1091/mbc.e07-10-1042